INSTITUTO TECNOLOGICO Y DE ESTUDIOS SUPERIORES DE MONTERREY

CAMPUS MONTERREY

Programa de Graduados de la División de Electrónica, Computación, Información y Comunicaiones

Optical router model under correlated and non-uniform traffic

THESIS

Presented as partial fulfillment of the requirements for the Degree of Master of Science in Electronic Engineering Major in Telecommunications

Ing. Job Josué Constantino Prado

December 2003

Optical router model under correlated and non-uniform traffic

by

Ing. Job Josué Constantino Prado

THESIS

Presented to the División de Graduados en Electrónica, Computación, Información y Comunicaciones

This job is a partial fulfillment of the requirements for the degree of

Master of Science in Electronic Engineering Major in Telecommunications

INSTITUTO TECNOLOGICO Y DE ESTUDIOS SUPERIORES DE MONTERREY

December 2003

INSTITUTO TECNOLOGICO Y DE ESTUDIOS SUPERIORES DE MONTERREY

DIVISION DE GRADUADOS EN ELECTRONICA, COMPUTACION, INFORMACION Y COMUNICACIONES

PROGRAMAS DE POSGRADO EN ELECTRONICA, COMPUTACION, INFORMACION Y COMUNICACIONES

The members of the thesis committee recommended the acceptance of the thesis of Job Josué Constantino Prado as a partial fulfillment of the requirements for the degree of Master of Science in:
Electronic Engineering Major in Telecommunications.

THESIS COMMITTEE:

PhD. Gerardo Castañón
Advisor

PhD. Cesar Vargas Rosales
Synodal

PhD. Juan Nolazco
Synodal

Approved

PhD. David Alejandro Garza Salazar
Director of the Graduate Program

December 2003

Dedicatory

To my parents, for giving me the life and impulse the initiated projects along it.

Thanks

Acknowledgements

To God, for giving me life, and this opportunity to keep going on, personal and professionally.

To my family, my father Luis Felipe, my mother María Isabel, my brother and sister, for always been beside me.

To my girlfriend Leonor, for supporting me every time.

To my friends, for its companion and help.

To the thesis committee for the support given for makeup of this thesis.

Thanks

Abstract

A detailed analytical traffic model for all-optical wavelength division multiplexing (WDM) photonic packet-switched router is presented and the requirements for buffer size are analyzed. Also it is known that due to the topology, packets may generate traffic bottlenecks produced by a tendency of the routing scheme to send packets with different destinations through preferred paths. This effect increases the traffic load and, hence, the probability of blocking at the output links of specific routers in the network and, therefore, a large buffer depth is required or an increment in the number of fibers per link. Furthermore, the relationship between traffic features at optical level and node modelling is addressed in order to outline analytical models to assess node performance. An analytical representation of traffic correlation, alongside with forwarding and buffering at switching nodes is discussed in order to support performance assessments such as packet loss probability. The statistical features, e.g. marginal distribution and correlation structure, of traffic reaching an output buffer in a time-slotted photonic packet switching node is investigated. Packet arrival patterns are generated through a well-known on-off analytical model with short-range dependence that accounts for packet forwarding as well. The purpose here is to find out how far the analytical model is from representing relevant characteristics present in self-similar traffic traces. An approach is proposed for modelling buffers under bursty traffic. Finally, is given a model for optical router with non-balanced input/output and correlated bursty traffic.

Contents

List of Figures

Chapter 1

Introduction

The development of optical fibers opened a new era in the history of telecommunications and the bandwidth availability, provided by this optical transmission medium, enabled the recent growth of new communication-based services. The increasing pressure on access network to provide broadband connections will initiate additional growth of data traffic from customers, which must be supported by the transport network (WAN and MAN). In principle, this continuous increase in traffic volumes is not an issue for the optical fiber itself, since its capacity has still to be fully exploited. However, it poses huge challenges for switching in transport networks. The problem is not only the volume of traffic to be switched but also the urgent need for traffic management strategies to be put in place.

Most of domestic and small businesses are still unable to afford the so-called broadband connections, and are restricted to interfaces bit rates much below the ones used in their LANs; therefore is now imperative to make available the bandwidth from backbones and thereby recover vast investments made recently in expanding its capacity. Conversions between optical and electrical domains might only happen at edge nodes of the optical network.

Telecommunications companies have been deploying transport network for the sole purpose of serving voice channels, transmission equipment are designed for this use. In order to build the widespread network that is the Internet today; circuits tapping into different levels of the transport network based on Synchronous Digital Hierarchy (SDH1,SONET) are leased by ISPs, organizations, and governments to interconnect their packet routers. ATM has been keeping, for the time being, its niche in WANs not only for its traffic management capability but also because it is able to transport non-best-effort services, e.g. VoIP. Deterministic multiplexing functions performed by SDH are not efficient for bursty data traffic. Datacom architects have envisaged the opportunity of using optical networks to solve some limitations of IP in WANs as well as creating a slimmer network stack by approaching IP to WDM.

Optical network is regarded as just one more layer where labels (packets header) may even correspond to wavelengths. Setting up a lightpath consists of mapping a particular pair input-wavelength to output-wavelength.

Another challenge is the nature of Internet traffic itself. High variability along with temporal correlation extending for very long periods has been detected nearly a decade ago from LANs [24] to WANs [32]. This effect is often called self-similarity due to the resilience of traffic variance regardless of the aggregation factor making buffering ineffective as a means of contention resolution when low packet loss probability is required.

One of the major problems in the design of all-optical packet-switching routers [4] is reduction of the number of components and the number of components a signal has to traverse without affecting the teletraffic performance of a network. The number of components in a router is driven by the degree of blocking probability desired. Packets may be lost when they contend for resources. Blocking occurs when two or more competing packets at the input of a router desire the same output. Buffering [35], multipath routing [6], wavelength translation [7], [2], and link dimensioning [8] are some of the techniques that can be used to solve the conflict of packets. Notice, however, that many solutions are possible by combining different amounts of each component in this three-dimensional space. Some cases studied in the literature are in Figure 1.1.

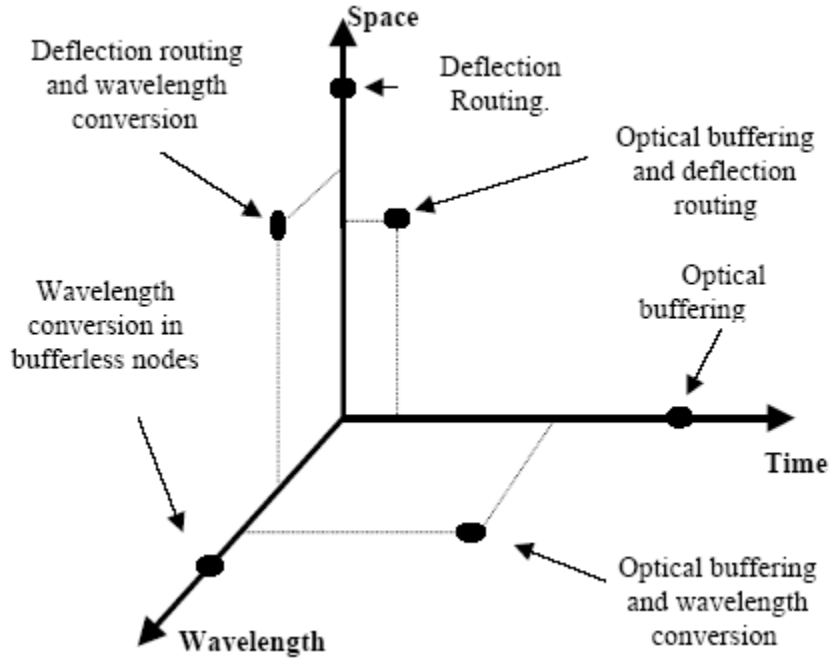

Figure 1.1: Contention resolution: three-dimensional space representation

The most utilized is buffering, which actually makes use of time domain, delaying contending packets until empty time-slots are available to proceed their transmission. Alternatively, contending packets could be routed through alternative links (deflection routing) to eventually reach their destinations provided there are on a connected network. Finally, the most recent proposal coming along with photonic switching technology is to change the wavelength a packet is carried upon. The teletraffic performance and the optimization of the number of components in a router have been analyzed assuming an isolated node [10]. Usually, a uniform distribution is assumed to assign the outlet destination to the incoming packets. The consequence of this kind of assumption

is that router architectures require a balanced buffer depth per outlet. Therefore, due to this assumption, the number of components used in the router increases. Due to the nonuniform network traffic behavior [9], routers require asymmetric buffering capacity to solve contention. Here is presented a wavelength division multiplexing (WDM) packet-switched router model that adequately represents the queueing behavior of the traffic in irregular mesh networks. Models that can effectively describe the behavior of the traffic in terms of a minimum number of parameters are of great practical significance. Several efforts have been demonstrated in [2] and [12] to model regular mesh networks under uniform traffic.

The information of the traffic matrix (source-destination load distribution), network topology, and routing tables, give us packet-forwarding probabilities of the routers, which are associated with routing in the node and consist of the proper selection of output wavelength and fiber both for transiting and for locally generated packets.

Router dimensioning is used to quantify the buffer size and the number of output fibers to achieve a specific probability of packet loss per router. We focus on two router architectures: the output optical buffers are completely partitioned (CP) among the outlets, and the shared buffer. The analytical results are compared to simulation results assuming correlated traffic. Also, we assume that the router operations are time slotted and synchronous, and fixed size packets are aligned at the node inputs. Each router performs access and routing functions. Access consists of the possible transmission of up to n wavelengths, of which the node is source. We assume full wavelength conversion, i.e., every packet can be converted to any of the available wavelengths.

1.1 Objective

The objective of this thesis is to develop an optical router traffic model under correlated traffic which takes into account load imbalances due to network topology, in order to analyze buffer performance.

1.2 Justification

There is already a network traffic model that consider independent traffic (packets) [5], and an electronic router model that considers correlated and imbalanced traffic [27], here is wanted to give an optical router model that can be included in a network model in order to manage correlated traffic considering load imbalances because of interconnections between all nodes in a network. This router model is not available yet in scientific literature. Also the traffic of today applications is highly correlated, such as Ethernet packets. The idea that routers analyzed be optical is due to there is no need to electronic conversion. That is what we expect for reducing costs in network and for exploitation of optical transparency (to transmission bit rate) .
All optical networks is expected to be in use during next future and this model will have direct applications to those networks, giving a really useful model.

1.3 Final Product

The final item is a model mentioned in the objective, and will be supported by simulations.

1.4 Summary

The present work is composed of five chapters, in the first chapter, we have the objectives and an introduction about what motivated the realization of this work. The second chapter is a background in which we talk about concepts like routing scheme and architecture, packet traffic characteristics. The third chapter has the router model, for traffic analysis, correlation and performance assessment for buffering, considering an isolated node. The fourth chapter considers an optical router model for correlated an non-uniform traffic. We conclude with the fifth chapter where conclusions and future work are given.

Chapter 2

Background

To begin with, we introduce fundamental concepts, their relation and the ones we concentrate.

2.1 Definitions

- **Dimensioning:** in general, it is a management function that solves the problem of assigning capacities to the resources such that for the given demand, the quality of service and performance metrics are within acceptable levels considering that the topology of the network and the external demand are known. Some of this resources may include the number of fibers, the number of channels per link, components such as router optical memories in the switching matrix, etc.
- **Irregular Network:** is a mesh network where nodes can have any input and output degree. A regular network is a mesh network where the nodes degree (input/output) is the same.
- **Transparent Network:** is a network where the main focus is to maximize signal transmission without electronic regeneration. Once interconnections are made optically, it is reasonable to think of a fully-optical central stage in order to eliminate expensive electrical/optical/electrical conversions and bit rate limitations. Ultimately, the same argument could be applied to input and output stages extending, as a result, optics from inlets to outlets making a transparent photonic switching node.
- **Optical Cross Connector (OXCN):** optical nodes that conduce traffic, with multiple inputs and outputs, it could be a router or switch.
- **WDM:** Wavelength Division Multiplexing, this implies multi-mode fibers.
- **Traffic source:** it can be a people making a phone call, an ON/OFF source can be a computer terminal connected to the Internet.
- **ON/OFF periods:** periods in which it is maintained or not, a phone call or a packet transmission.

2.2 Routing scheme and router architecture

Optical packets must be routed through a network from the origin and through intermediate nodes (OXCN) to reach the destination. The general optical WDM network which we consider is shown in Figure 2.1. It is a mesh network in which signals on n different wavelengths, $\lambda_1 ... \lambda_n$, are used to carry cell traffic between the optical network nodes.

Wavelength division multiplexing (WDM) has been proposed as a way of increasing the capacity in future optical networks. Furthermore, WDM networks are likely to use optical switching to avoid the bottlenecks of electronics as well as to increase the transparency of optical networks. The absence of an effective way to store cells in the optical domain, reduces the realistic buffer capacity of optical packet switches. The optical buffer is realized by fiber delay-lines. By exploiting the wavelength dimension, using WDM and employing tuneable optical wavelength converters (TOWC's), the required number of fiber delay-lines in optical packet switches can be reduced.

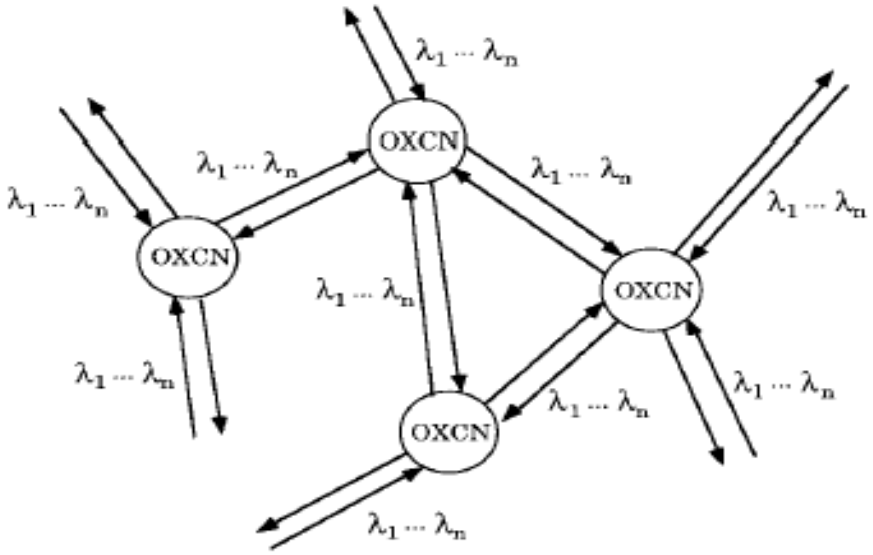

Figure 2.1: WDM WAN Backbone Network

The decision of the path to be followed is made by a control unit, which most often is implemented with electronic techniques. The routing algorithm is closely related to the network topology and, thus, to the type of switching routers in use. Routers in irregular meshed networks use predefined lookup tables to forward- arriving packets. Usually, a shortest path or least number of hops algorithm is used to define the optimum output at every router in the network. There is normally a single path and, therefore, one output for every packet that arrives to the router. Analysis of the router performance in terms of packet loss, number of delay lines, size of the router, and number of wavelengths has been studied for the case of single-path routing and uniform-router traffic [10]. The router architecture, demonstrated in [11], is the architecture used in this analysis and is shown in Figure 2.2.

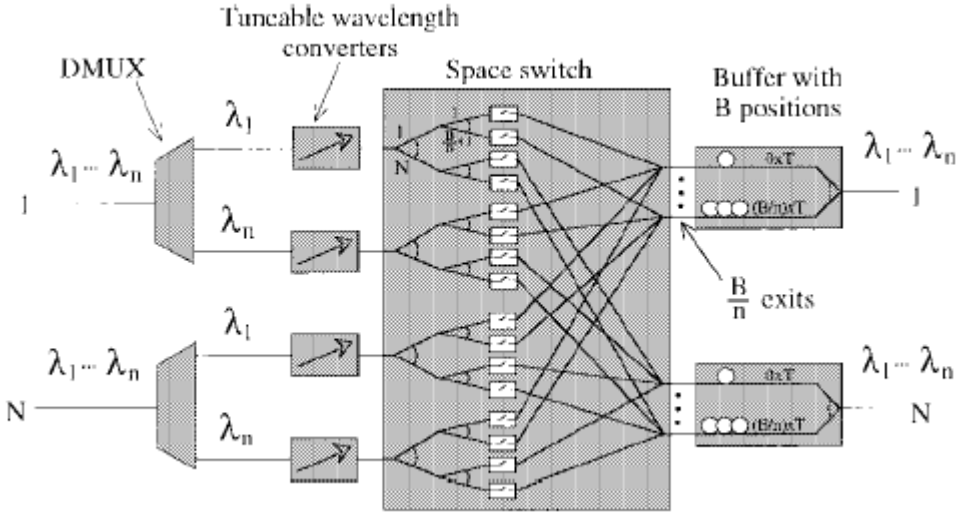

Figure 2.2: WDM packet switch with buffers realized as fiber delay-lines and with tuneable wavelength converters to address free space in the buffers. T corresponds to the duration of a packet.

The demultiplexer (DEMUX) selects the packets arriving on wavelengths $\lambda_1, ..., \lambda_n$, on each of the N input fibers. Optical- to-electrical interfaces located after the DEMUX are used to read the packet headers by which the destination and thereby switch outlet can be found. Also, after the demultiplexer, tunable WCs are utilized to solve blocking of packets by addressing free space in the fiber delay-line output buffers. The space switch consists of optical gates that control the flow of packets to the designated output and fiber-delay lines in the output buffer, the size of the space switch is $Nxn \cdot N(B/n)$. Fiber-delay lines provide the packet buffering and are present at the output of the router [10]. In Figure 2.2, B is the number of cell positions in the buffer, n is the number os wavelengths, N the number of in- and out-lets and B/n the number of fiber-delay lines, each capable of storing n packets. There is at least one inlet to inject up to n packets into the network and at least one outlet to absorb up to n packets from the network. Logically, the router has the functions of packet dropping (absorption), adding (injection), wavelength switching (conversion), routing (space switch), and buffering. Observe that architecture in Figure 2.2 has completely partitioned buffers because fiber-delay lines are distributed among the outlets.

In Figure 2.3 we see the physical layout of fiber delay-line buffer architecture. Architectures with buffers dedicated to each outlet require a smaller number of wavelengths in comparison to shared buffers. Efforts must be gathered towards understanding traffic features in order to keep the buffer depth as low as possible. Noise accumulation, power splitting, fiber non-linearities, crosstalk, amplitude and phase fluctuation in the switch fabric are some of degrading effects taking place at physical layer. The performed analysis here considered does not take into account influences of physical layer on packet loss performance.

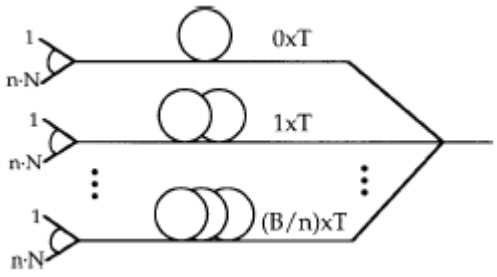

Figure 2.3: Physical layout of fiber delay-line buffer architecture. B is the number of cell positions in the buffer, n the number of wavelength channels per in- and out-let, N is the number of physical in- and out-lets while T is the duration of a cell.

2.3 Traffic of packets at electronic layers

Teletraffic theory is being changed to a great extend during the last decades. It is often argued that models that were extensively used in telephony do not account for features of today's data-oriented network. Telephony network uses circuit-switched technology and traffic is basically modelled as Poisson arrivals (connection requests) and exponential holding time per connections; leading to what is called Erlang distribution for blocking probability when establishing a new connection [28]. Hence, one is able to properly design network elements that are to be shared by many subscribers, e.g. switching centers modules and trunk lines. In packet switched networks, on the other hand, the aim is to design buffers with the purpose of reaching an acceptable packet loss probability by solving packet contention.

Temporal correlation between packets has been one of salient feature present throughout the history of packet switching technology. The first efforts to model the bursty behavior of data networks let to the concept of packet trains discussed in [23]. Comprehensive statistical characterization studies were pursued in [25] until a major breakthrough happened in early 90s when Long-Range Dependence (LRD), also known as self-similarity, has been identified in Ethernet traffic [24]. Self-similarity could be summarized as follows. The observation of traffic sources indicates a very large variance associated to the amount of traffic generated. In addition, this traffic possesses high levels of time-correlation spreading across long periods. Consequently, the effectiveness of buffering in reducing packet loss (due to contention) is considerably weakened and so is the aggregation at the core network of the photonic router as a means of smoothing traffic variance and improving link utilization.

2.3.1 Burstiness

A bursty traffic source is one that generates traffic in (random) clusters. Bernoulli traffic have clusters of traffic and is more bursty than a deterministic source. However because this perceived burstiness can be smoothed through aggregation (unlike self-similar soruces) bernoulli traffic is not considered to be truly bursty [36].
When several sources are supplying bursts of packets at the same time, the load is thus larger and queue length increases (with respect to non bursty sources), the tail probability for buffer

occupancy decreases slowly (instead of linear decrease). A buffer size of B may be sufficient to achieve a certain probability of packet loss if traffic is non-bursty but would be too small for bursty traffic. Thus larger buffers will be needed if sources are bursty in order to achieve the same buffer occupancy performance level.

2.3.2 Causes of long-range dependence

In voice connections generally one part speaks while the other remains mute. Therefore, the production of packets is a clear alternation between bursty and silent periods. It is perfectly foreseeable that this dependence is expected, on average, not to last for very long time span once it is due to the bursty nature of human conversation itself. This leads to temporal-correlation among generated packets that, in contrast with voice over packets, may persist over very long periods of time.

2.3.3 Traffic features

The statistical background to understand the features of modern traffic sources is briefly discussed here. It has two basic objectives: to clarify the relevant issues on traffic characterization, and to introduce few basic mathematical tolls used for trace analysis in this work.

2.3.4 Section arrivals and duration, packet inter-arrival time, arrival counting, and heavytailness

Arrival of section requests can be still modelled as Poisson arrivals just like connection requests in telephony for human generated requests such as telnet and FTP [32]. However, sections time distribution on the Internet, whatever origin, presents slow decay. This contrasts with connection duration (holding time), well represented by exponential distribution in telephony. This sort of probability distribution is often called heavy-tail and is defined as in

$$Prob\{U \geq u\} \approx u^{-\alpha} L(u) \text{ as } u \longrightarrow \infty \text{ and } \alpha > 0 \tag{2.1}$$

with $1 \leq \alpha \leq 2$ and $L(u)$ being a slowly-varying function (e.g. logarithm or constant such as $lim_{t \longrightarrow \infty} L(tx)/L(t) = 1$). One may interpret Equation (2.1) as follows: most connection lasts very little but the bulk of the traffic volume is composed by few long-living connections [38]. Another consequence of heavytailness associated to section duration is that the longer the period of observed activity, the more certain that it will persist into the future [30]. In light-tail distributed process (such as exponential) the expected duration is the same regardless of its elapsed time. The IP network is not slotted in time. As a result, some prefer to associate the high variability of heavy-tail distributions to the interval between arrivals (inter-arrival time). On the other hand, for ATM traffic, which works on a slotted-time basis, the variance is often related to the number of arrivals (or amount of bytes) in a multiple of the time-slot interval. Traffic will be regarded as a time-discrete stochastic process $X(t)$ comprising arrivals (e.g. bits, bytes or packets) per time interval. It must be said that the heavy-tail feature does not necessary imply self-similarity

2.3.5 Stationarity

A discrete stochastic process $X(t)$ is considered stationary whenever its joint statistical features for any set of samples are all the same regardless of the time-reference frame adopted for observation. Under a less restrictive definition, if at least the two first moments are time-invariant, one may define the autocorrelation coefficient $r(k)$ using $\mu_X = E[X]$ and $\sigma_X^2 = E[(X-\mu)^2]$ as the mean and variance, respectively as follows

$$r(u,v) = E[(X_u - \mu)(X_v - \mu)]/\sigma_X^2 \tag{2.2}$$

$$r(u,v) = r(u+k, v+k) \qquad u,v,k \in \{0,1,2,...\} \tag{2.3}$$

$$r(u,v) = r(0, u-v) = r(k) \tag{2.4}$$

If the autocorrelation function also satisfies the translation invariance, leading to the autocorrelation function being defined only by the relative difference between temporal samples as in Equation (2.4), this process is classified as wide-sense stationary (also known as second-order stationarity) [28].

2.3.6 Long-range dependence and second-order self-similarity

A wide-sense stationary process $X(t)$ is long-range dependent (LRD) if $r(k)$ is non-sumable (i.e. $\sum_k |r(k)| \longrightarrow \infty$), meaning that samples are still related to each other no matter how far apart they are, which means that correlations decay to zero so slowly that they are not sumable. An exact (second order) self-similar process is characterized by the Hurst factor H ($0.5 < H < 1$) shown in Equation (2.5), that is the Autocorrelation Coefficient of Fractional Gaussian Noise Process, which represents the self-similarity phenomenon [1].

$$r(k) = \begin{cases} [(k+1)^{2H} - 2k^{2H} + (k-1)^{2H}] & 0 < k < \infty \\ 1 & k = 0 \end{cases} \tag{2.5}$$

Experimental measurements can be compared with Equation (2.5) for identification of LRD in traces. For a finite number of samples, say Z, the correlation coefficient can be obtained as in Equation (2.6)

$$\hat{r}(k) = \frac{\sum_{i=1}^{Z-k}[X(t_i - \hat{\mu}_X)][X(t_i - t_k) - \hat{\mu}_X]}{(Z-k)\hat{\sigma}_X^2} \tag{2.6}$$

where $\hat{\mu}_X$ and $\hat{\sigma}_X$ are temporal mean and (unbiased) variance estimation from the finite traffic trace calculated as shown in Equation (2.7) [28]

$$\hat{\mu}_X = \frac{1}{Z}\sum_{i=1}^{Z} X(t_i) \qquad \hat{\sigma}_X^2 = \frac{1}{Z-1}\sum_{i=1}^{Z}[X(t_i) - \hat{\mu}_X]^2 \tag{2.7}$$

By increasing the observation window (time-scale) in which a stochastic process is analyzed, one may see the effects of long-range dependence manifesting its graphical fractal-like behavior. This is due to the slow reduction of variance as the process is viewed in coarser scales. A convenient way to

assess this (and estimate the Hurst factor) is by constructing a new stochastic process comprising of non-overlapping blocks of $X(t)$ containing $m \in \{1, 2, ...\}$ samples as shown in Equation (2.8).

$$X^{\{m\}} = \frac{1}{m} \sum_{i=tm-m+1}^{tm} X(i) \tag{2.8}$$

Each block produces a single sample by averaging m samples of the original process. This is somehow equivalent to observing $X(t)$ in a time scale that is m coarser than the original. Notice that $lim_{m \longrightarrow \infty} X^{\{m\}} = \mu_X$ consequently $\sigma^2_{X^{\{m\}}} \longrightarrow 0$ as m increases towards infinity. Plotting the new variance against the aggregation factor using a log-log scale, one can use the slope (S) for Hurst parameter estimation $\hat{H} = (S + 2)/2$, although this method does not allow interval of confidence measurements. It is worth looking at the two extreme values for H, with $H \longrightarrow 0.5$ the variance of $X^{\{m\}}$ reduces at the same rate m increases, which actually means that the stochastic process is completely uncorrelated. This lack of correlation can be confirmed by the fact that in Equation (2.5) where $r(k) = 0$ for $H = 0.5$ and $k > 1$, meaning that no self-similarity will be present as the time scale of observation is increased and the variance is quickly smoothed by aggregation. On the other hand, for $H \longrightarrow 1$ the variance stays virtually the same regardless of the aggregation factor m. This is explained by the autocorrelation $r(k) = 1$, $\forall\ k$.

The process X is exactly second order self-similar if for positive integer m, are satisfied Equation (2.9) and (2.10)

$$VAR(X^{\{m\}}) = \sigma^2 m^{-\gamma} \quad 0 < \gamma < 1 \tag{2.9}$$

$$r^{\{m\}}(k) = r(k) \qquad k \geq 0 \tag{2.10}$$

for which, the Hurst parameter H is given in Equation (2.11)

$$H = 1 - \gamma/2 \tag{2.11}$$

The process X is called asymptotically second order self-similar if for all k large enough, is satisfied Equation (2.12)

$$\lim_{m \longrightarrow \infty} r^{\{m\}}(k) \longrightarrow r(k) \tag{2.12}$$

where $r(k)$ is given by Equation (2.13)

$$\lim_{k \longrightarrow \infty} r(k) \approx k^{-\gamma} L(t) \tag{2.13}$$

self-similarity also implies variances decay slowly as in Equation (2.14)

$$\lim_{m \longrightarrow \infty} VAR(X^{\{m\}}) \approx c m^{-\gamma} \tag{2.14}$$

where c is a constant.

In summary, the aggregated version depends upon the correlation structure of the original samples. Therefore, long-range dependence implies (second order) self-similarity. In other words, if samples are strongly related to each other the aggregation will result in a process very similar

to the original one (in distribution). This also explains the presence of self-similarity MANs and WANs since aggregation does little to decrease variance when sources bear long-range dependence.

2.3.7 Statistics for aggregation in time

Let $X(t)$ represent the evolution in time of the volume of incoming traffic. This stochastic process produces random variables $X1$, $X2$, ... when sampled at a given regular time-interval $t = t1$, $t = t2$ ... respectively. The aggregation of m samples so that $F = X_1 + X_2 + ...X_m$, produces a sample of $\Theta(t)$ which represents the evolution of the aggregated traffic, where m the number of time-intervals collected from the original stochastic process. The expectancy (ensemble average E[.]) of this aggregation is a straightforward multiplication, shown in Equation (2.15), of the original expectancy by the number of samples that has been grouped regardless of statistical dependence [14].

$$E[\Theta] = mE[X] \tag{2.15}$$

However, the general calculation for variance, here represented by Var[.], is given by the summation of the autocovariance matrix [26] composed of m x m elements, that is, the summation all combinations of m elements in the correlation coefficient, as stated in Equation (2.16).

$$var[\Theta] = \sum Cov_{xx} = var[X] \sum_{u=1}^{m} \sum_{v=1}^{m} r(u, v) \tag{2.16}$$

If arrivals are uncorrelated, the correlation coefficients are null except for $u = v$. Therefore the variance grows linearly with m as $u = v$ is satisfied m times. In the case of a wide-sense stationary and exact (second order) self-similar process, one may use the autocorrelation function given in Equation (2.5) and substitute it in Equation (2.16). Realizing that $r(u, v) = r(|u - v|)$ due to the wide-sense stationarity, the double summation produce m occurrences of zero, and $2(m - k)$ of each value of k ($k \in \{1, 2, ..., m - 1\}$), the time-aggregation variance is then calculated as in Equation (2.17).

$$var[\Theta_i] = var[X_i]\{m + \sum_{k=1}^{m-1} (m - k)[(k + 1)^{2H} - 2k^{2H} + (k + 1)^{2H}]\} = var[X_i]m^{2H} \tag{2.17}$$

The simple relationship between variance and aggregation revealed by Equation (2.17) is at the root of self-similar stochastic processes. An exact (second-order) self-similar process proportionally maintains its variance, according to the Hurst factor, regardless of the observation interval. Although the proof of Equation (2.17) is trivial (see Appendix). So, it is shown the equivalence of Equation (2.16) and Equation (2.17), named covariance matrix and self-similar property respectively, for an exact (second-order) self-similar process. Variance-plot performs gathering in time from the original trace but instead of simply collecting arrivals, variance-plots use a mean value, i.e. multiply the aggregate by $1/m$. As a result, the variance of new samples is the variance of the aggregate times $1/m^2$.

2.4 Traffic models for node performance evaluation

The relationship between packet arrival patterns and outputs they are forwarded to has strong influence on node performance and therefore modelling must account for it as accurately as possible. Effects such as bursty arrivals, hot-spot, and temporal/spatial correlation and contention in nodes operating under time-slotted system are illustrated in Figure 2.4. The numbers inside the packets represent outlet ports used to despatch them. Assuming that the node shown in Figure 2.4 is only able to forward one packet per output in a time-slot, arrivals beyond this limit have to be either discarded or treated by a technique of contention resolution discussed above. For instance, packets arriving in the sixth time-slot on input 1 and 4 are contending for the same output. In addition, notice that packets on inlet 4 arrive in a cluster of three packets all destined to output 3 while the burst(various packets in sequence) on input 1 has packets headed for different outlets. In case packets are arriving in such clusters on a regular basis, time-correlation feature is present in the arrival pattern. This correlation may last for few time-slots or even go through very long periods of time. It has been shown that temporal correlation has a major influence on decreasing buffer efficiency in reducing packet loss probability [13][17][21][31][37]. Moreover, a given port (or a group of them) may receive, on average, more packets than the reminder ports. In the illustrative example given in Figure 2.4, traffic loads on inlets 1 and 4 are higher than on 2 and 3 while outlets 3 and 4 receive most of the arrivals. These traffic imbalances (also known as hot-spots) certainly pose more complex challenges to the mechanisms of contention resolution. The more packets are headed for a given output the fewer are destined to the remainder for a switch with finite number of inputs.

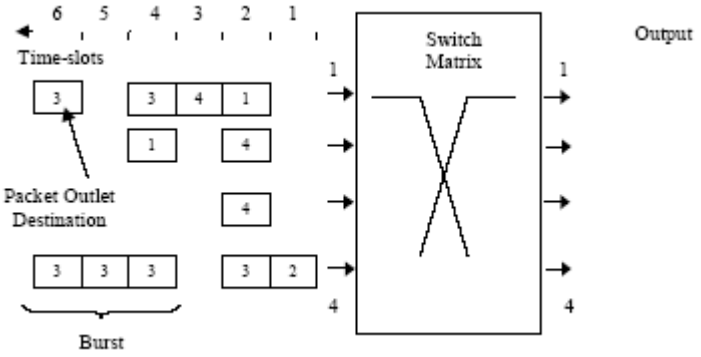

Figure 2.4: Traffic Features: Arrival Patterns.

It is not difficult to conclude that many interrelated phenomena have to be taken into account for modelling traffic features and forwarding in order to evaluate node performance properly. Ideally, packets in transit on a network must arrive to the destination node as soon as possible and should not be lost. However, due to the intrinsic nature of this kind of switching technology, this packet may have to contend for the same resources with other packets at some node in the path between source and destination. As a result, some packets have to wait in buffers, follow different paths or even have to be discarded. Therefore, a basic metric to evaluate packet switching nodes must involve the rate packets are lost due to contention.

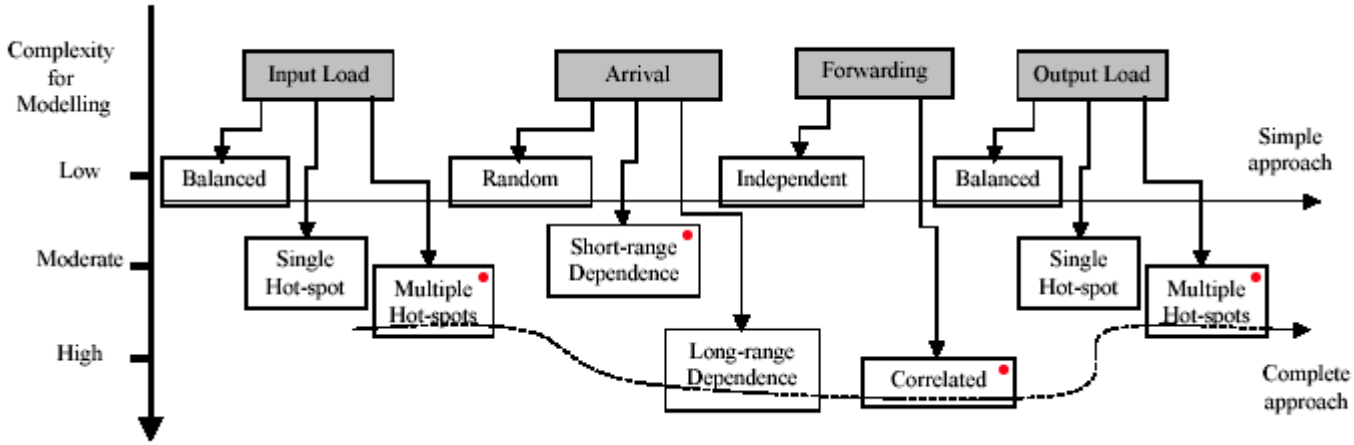

Figure 2.5: Traffic Features: Classification and complexity.

2.4.1 Model complexity

An illustrative classification system comprising traffic features and forwarding model for packet switching nodes is presented in Figure 2.5. There is also a vertical scale indicating the complexity associated with the modelling of various traffic characteristics at different node parts. The common sense indicates that the more complex is the model the closest to the real behavior it becomes. Therefore, limit approaches could be devised, named here simple and complete. For the former, one may develop a model to evaluate node performance considering the incoming traffic as totally uncorrelated (random) and packets evenly distributed among outlets (independent forwarding). On the other extreme, there is a complete model that would include long-range temporal correlation in the incoming traffic representation. This kind of traffic often produces bursts that are composed of packets going to the same output. Therefore, correlated routing must be considered in order to model the routing of those bursts accordingly; otherwise independent forwarding would alter the correlation structure.

Notice that the analytical effort that must be put into the development of the complete model can be prohibitive while the simplest model might produce results of little practical interest. Nonetheless, this dilemma may be avoided when one considers that there is a whole range of options in between these two extreme models that could well produce reasonable results. A compromise solution between performance and model complexity might be archived by choosing only relevant aspects in describing the problem under study. For an output buffered node, the fact of having an incoming correlated and non-balanced traffic is completely irrelevant unless the packets are to be forwarded to the same output. In conclusion, a fairly simple analytical model accounting for short-range dependence with correlated forwarding and balanced loads (input and output) may produce acceptable traffic characterization for output buffered photonic nodes.

The relative importance of performance metrics is entirely up to the application. Real-time services, e.g. telephony, may be sensitive to delay while mission-critical applications, e.g. exchange

of control/management information, must rely on nodes with very low packet loss probability. Moreover, the metrics mentioned above are generally taken from first-order statistics of a stochastic process. Therefore, one may have to consider different metrics for different applications that utilize the packet network to transport information. Nevertheless, the analysis performed in this works considers first-order metrics only.

2.4.2 Analytical and numerical models

Analytical models are complex and time-consuming to develop. In addition, assumptions and simplifications have to be made in order to keep its analytical tractability. Numerical models, on the other hand, can significantly reduce analytical effort with the advantageous feature of better description of the real problem. The downside, however, lies in the prohibitively long time taken to assess performance indicators such as low packet loss probability levels (e.g. 10^{-7} and below). New simulation techniques, such as faster processors may keep on tilting the balance in favor of numerical solutions. Nevertheless, proper validation of numerical results is troublesome, as many outcomes are necessary in order to improve the interval of confidence of such results [28]. Alternatively, simplified analytical model can at least as performance, bounds providers in validating numerical methods and results. Conversely, few time-consuming computations using numerical models are often used to endorse analytical approaches that, once validated, are ready to be extensively used to, for example, assess low packet loss probabilities.

Chapter 3

Router Model

In this chapter we turn into the router model under correlated traffic.

3.1 Analysis of traffic forwarding and buffering for node performance assessment

An analytical representation of traffic correlation, alongside with forwarding and buffering at switching nodes, is discussed in this Chapter in order to support performance assessments such as packet loss probability. The statistical features, e.g. marginal distribution and correlation structure, of traffic reaching an output buffer in a time-slotted photonic packet switching node is investigated in the first part of this Chapter via analysis and simulation. Packet arrival patterns are generated through a well-known on-off analytical model with short-range dependence that accounts for packet forwarding as well. The purpose here is to find out whether traffic features of such a simplified analytical approach are equivalent to all-inclusive numerical models and how far it is from representing relevant characteristics present in self-similar traffic traces. Results indicate that the model under analysis is accurate and may even produce more severe test conditions to buffering than self-similar traffic. The understanding developed helps interpreting results from the second part of the Chapter, which deals with the analysis of performance when the traffic finally goes through buffers. A generic and exact approach is proposed for modelling buffers under bursty traffic.

3.2 Introduction

Performance estimation through mathematical models plays a central role in the design of present communication systems. The future photonic packet switching network will be no exception. However, a better understanding of traffic that will be processed by such nodes is still needed. The design of fundamental functions, e.g. contention resolution through buffering, depends upon this knowledge. It is often argued that traffic temporal correlation represented through models with Short-Range Dependence (SRD) is an obsolete method, since modern traffic sources actually possess long-range dependence (LRD) in their correlation structure. Nonetheless, one should seek a balance between simplicity and accuracy regarding the models utilized to represent the physical

entities involved in the analysis of performance.

A simple illustration is given in Figure 3.1 for the case analyzed in this Chapter. The number of delay-lines provided to sort out contention is represented by b. Each wavelength (sometimes referred as channel in this work) is loaded at ρ ($0 \leq \rho \leq 1$) which can also be interpreted as the probability of finding a busy time-slot. *Each source is assumed to have identical load.* The major concerns of this Chapter are:

- to model traffic generation and understand the traffic features reaching an output node. The traffic in this case is composed by sections of traffic coming from N inputs (each of them bearing n wavelengths) that are forwarded to the observed output. *The analysis will be focused on any one particular output line.*
- to assess the effectiveness of buffering under both uncorrelated and correlated traffic.

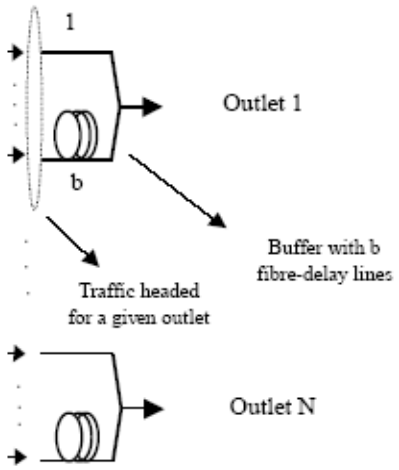

Figure 3.1: Illustration for output buffering and main issues discussed in this Chapter

This Chapter looks into traffic features of a simple model (bursty on-off) that is able to take into account correlation features at arrival and forwarding levels and is particularly suited for output buffered nodes, like the one considered in this job. Marginal distribution, correlation structure, load distribution, and aggregation features are the characteristics studied via analysis and numerical simulation. Another point to be discussed here is to what extend claims that this sort of model overestimates node performance, due to the lack of LRD, are consistent. The detailed understanding developed here paves the way for performance assessment of nodes using output buffers under traffic with and without time correlation (and tuneable wavelength conversion). A well-known approach for modelling uncorrelated traffic buffering is initially presented to be generalized for the case of time-correlated arrival. If a given performance target is to be met, the traffic features and number of wavelengths utilized will dictate buffer depth which also affects switch matrix cross-point count as packets have to be directed to b elements in order to reach outlet without conflict.

3.3 Previous work

Analytical models representing traffic temporal-correlation with SRD have been in use since first investigations of voice over packets, e.g. [15] [16]. After the introduction of Asynchronous Transfer Mode (ATM) technology, these models have been extensively studied and upgraded in the view of new traffic sources bearing temporal correlation using this multimedia-oriented transport platform. There are two basic areas of study regarding the analytical model in this area. The first concerns the modelling of traffic sources themselves while the second addresses the transit and buffering of packets in switching nodes, involving the understanding of traffic gathering at outlets due to packet forwarding process and its influence on buffering performance. Studies analyzing traffic superposition of correlated sources can be found in [22], [29], and [39] while investigations into buffer performance are carried out in [3], [18], [19], and [27].

The study presented in this Chapter is based on model for source representation and traffic forwarding developed in [19] while buffer modelling and performance from [10], which is a generalization from [18] for use of TWC/WDM. This Chapter uses [3] to extend the model developed in [10] providing an exact and clear solution for performance evaluation of correlated traffic. Regardless of being a widely used model, little is known about traffic features produced by this method regarding the relevance of various factors that compose traffic statistics reaching output buffers. The validity of such a model when LRD is present, instead of SRD, needs to be assessed.

3.4 Model for packet source and forwarding

Next, it is shown the model for the traffic sources and the forwarding process for allocating incoming packets to a given destination.

3.4.1 Source model

The model considers the input traffic per wavelength as a two-state system, more specifically High and Low for the representation used in Figure 3.2. Sources are independent and identically distributed (i.i.d.) and they are either producing a continuous stream of packets while in High state or no traffic at all during Low state (or generating packets for other outputs). The synchronism of the network ensures that all packets arrive at the beginning of the time slots [20]. The transition probabilities R_{HL} and R_{LH} stand for High to Low and Low to High respectively. Each source emits intermittently bursts of consecutive packets, where the burst length l is geometrically distributed (geometric source) according to

$$l(i) = \begin{cases} R_{HL}R_{LH}^{i-1} & i > 0 \\ 0 & \text{otherwise} \end{cases} \tag{3.1}$$

Each source spends, on average, $1/R_{LH}$ on Low state and $1/R_{HL}$ time-slots on High state. The latter is the mean burst length β, also known as burstiness. Applying local balance boundary to the source model shown in Figure 3.2 one finds Equation (3.2) as demonstrated in the Appendix.

$$Prob[state = High] = R_{LH}/(R_{LH} + R_{HL}) \tag{3.2}$$

3.4.2 Forwarding model

Balanced input and output loads are assumed. The forwarding process considers that, in the long term, the incoming traffic is equally distributed among the output ports. An ingenious way is utilized in [19] to addresses forwarding via a hybrid representation between independent and correlated approaches discussed in previous Chapter. This is done by evenly distributing the input load among outputs in the long term but each burst generated is forwarded in a correlated way to a given output. Consequently, one only needs to keep track of sources addressed to the tagged output. As packets are exclusively released in the High state, $Prob[state = High] = \rho/N$ and from Equation (3.2) the probability of transition from Low to High can be calculated as stated in Equation (3.3)

$$R_{LH} = \left(\frac{\rho}{N} R_{HL}\right) / \left(1 - \frac{\rho}{N}\right) \tag{3.3}$$

Temporal evolution for the number of sources in High state addressed to the tagged output is modelled by a Markov chain, illustrated in Figure 3.2, in which any transition among the $S_i (0 \leq i \leq nN)$ states is allowed.

For each source, the transition probabilities are taken as geometric distributed with mean R_{HL} and R_{LH} for sources leaving state H and state L respectively. As a result, the number of input sources in state H and addressed to the outlet under observation in a given time slot is a binomial distribution, where i represents the current number of sources in High state while j also stands for that quantity a time-slot ahead. An auxiliary variable z is brought in to represent all possible combinations regarding transitions of individual sources, finally allowing the calculation of transition probability from i to j $(i, j \in \{0, 1, ..., nN\})$ in a compact expression [19] as shown Equation (3.4).

$$Q_{ij} = Prob[S(T+1) = S_j \backslash S(T) = S_i] = \sum_{z=max(0,i-j)}^{min(i,nN-j)} \Delta L(z,i) \Delta H(z-i+j, nN-i) \tag{3.4}$$

$$\Delta_L(u,v) = \binom{v}{u} R_{HL}^u (1-R_{HL})^{v-u}; \quad \Delta_H(u,v) = \binom{v}{u} R_{LH}^u (1-R_{LH})^{v-u}$$

The resulting arrival pattern, represented here by a discrete stochastic process $A(t)$, at a given output is the summation of individual contributions in each time-slot as illustrated in Figure 3.3 for three inputs that have packets addressed for the tagged outlet. The marginal distribution and two random variables from temporal samples of such a stochastic process A_τ and $A_{\tau+k}$, (taken at $T = \tau$ and $T = \tau + k$ respectively), are also shown.

3.5 Marginal distribution

Two methods for obtaining the marginal distribution for traffic reaching an output buffer are discussed here, namely, steady-state solution for the Markov chain representing state of input sources, and convolution of individual contributions within a time-slot.

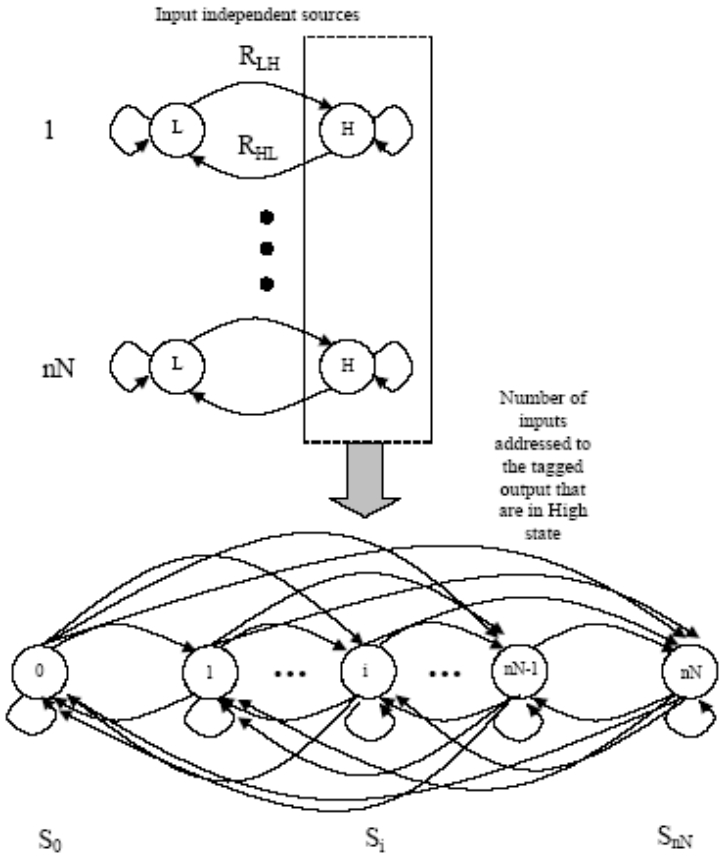

Figure 3.2: Analytical model. (a) Source representation.

3.5.1 Analysis via Markov chain

The steady-state solution for the temporal evolution of number of sources in High state can then be found by solving the Equation system presented in Equation (3.5). The underlined S and q are the state and transition probabilities, in vector and matrix form respectively; e is a unitary column vector, i.e. $e = [11\ldots1]^T$, with nN+1 elements while $\star$ stands for matrix product.

$$\begin{cases} \underline{S} = \underline{S} * \underline{\underline{Q}} \\ \underline{S} * \underline{e} = 1 \end{cases} \tag{3.5}$$

Once packets are released with probability 1 ($\mu_H = 1$) for sources at High state, vector S may be seen as the marginal distribution for the discrete-valued stochastic process $A(t)$, i.e. $S = p_A(a) = Prob[A = a], a \in \{0, 1, 2, ..., nN\}$.

3.5.2 Analysis via Central Limit Theorem (CLT)

Provided that the traffic addressed to a given output is simply a summation of independent random variables $\varpi^{\{i\}}$, with $\varpi \in \{0, 1\}$ which are temporal samples from $\xi^{\{i\}}(t)$ coming from $i \in \{1, 2, ..., nN\}$ inputs within a time-slot as shown in Figure 3.4, one is able to find out the

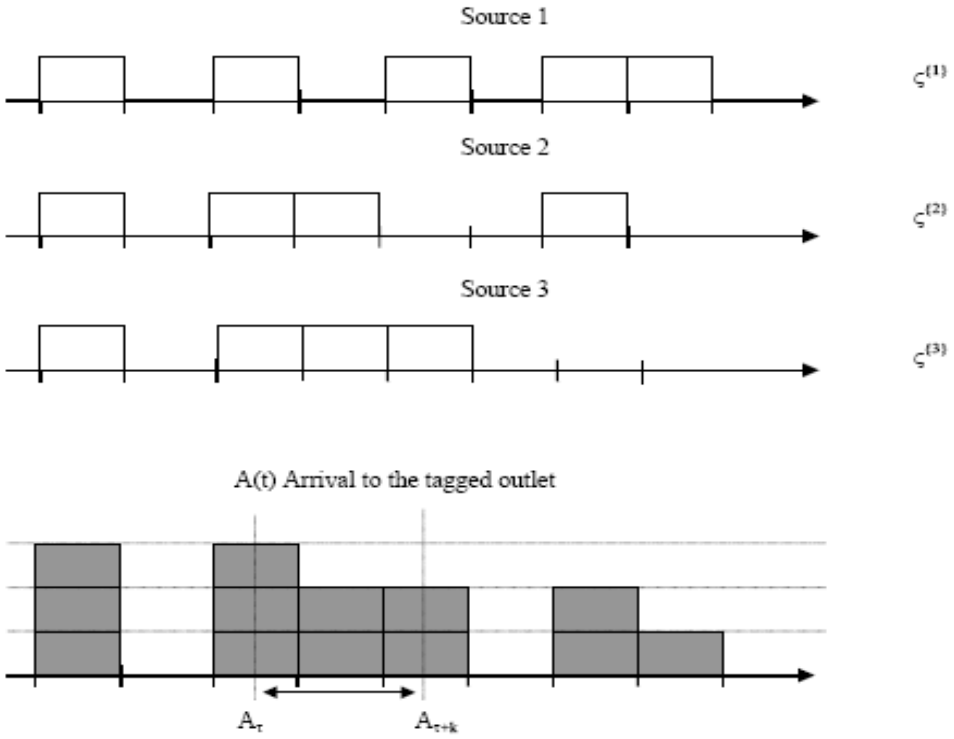

Figure 3.3: Analytical model. (b) Illustration for traffic reaching an output buffer.

marginal distribution at the outlet under analysis by convoluting (convolution is represented by the symbol $\otimes$) the individual contributions from each input as stated as follows

$$P_A(a) = P_\varsigma^{\{1\}}(\varpi) \otimes P_\varsigma^{\{2\}}(\varpi) \otimes \cdots \otimes P_\varsigma^{\{nN\}}(\varpi) \tag{3.6}$$

For the assumptions that have been made, the probabilities of sending either one or no packet to the tagged output is given by Equation (3.7). One should expect this distribution to go through intermediate profiles, e.g. Poisson-like, while with a limited number of sources before reaching Gaussian shapes for $nN \longrightarrow \infty$.

$$P_\varsigma(0) = Prob[\varpi = 0] = \left(1 - \frac{\rho}{N}\right); \quad P_\varsigma(1) = Prob[\varpi = 1] = \frac{\rho}{N} \tag{3.7}$$

Analyzing CLT under balanced load presented and i.i.d. sources in Equation (3.7) and Equation (3.6) one can find Equation (3.8).

$$P_A(a) = \binom{nN}{a} \left(\frac{\rho}{N}\right)^a \left(1 - \frac{\rho}{N}\right)^{nN-a} \tag{3.8}$$

Although the binomial distribution in Equation (3.8) is widely used, e.g. [10] [18], calculations using Equation (3.6) allow generalized cases, such as forwarding hot-spot, to be analyzed. Moreover, it provides a proof for the memoryless nature of the marginal distribution despite the presence of time correlation in each source composing the total arrivals.

3.6 Correlation structure

It is of great interest the correlation structure present in such aggregation of time-correlated but independent sources. An exact and simple method is developed to perform this investigation. In addition, an analytical calculation to obtain variance-plot charts is also introduced.

3.6.1 Correlation coefficient function

Provided that $A(t)$ is a stationary process, the two samples k time-slots apart, $k \in \{1, 2, ..., \infty\}$, A_0 and A_k, have the same marginal distribution $p_A(a)$ but they may not be independent. In order to evaluate the correlation coefficient between them, the joint probability density $p_{Ao,Ak}(a_o, a_k)$ is needed. Figure 3.4 illustrates the relationship between time samples that is exploited in order to calculate the joint probability. The arrows represent transition probabilities given by Equation (3.4).

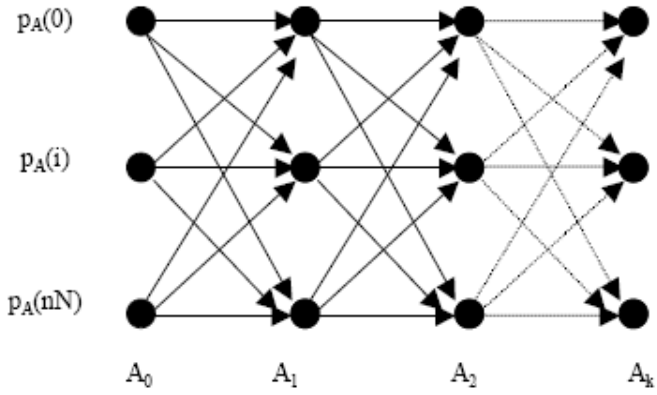

Figure 3.4: Correlation coefficient analytical calculations

The joint density is then obtained by multiplying $p_A(a)$ by the conditional probabilities of transition (given by Q) for each step forward in time. If Q is stationary this may be represented as in Equation (3.9) where $(\cdot)$ stands for scalar product and PP is a square matrix composed $nN + 1$ repetitions of $p_A(a)$, as shown in Equation (3.10).

$$\underline{\underline{P_{A_1 A_k}}} = \underline{\underline{PP}} \cdot [\underline{\underline{Q}}(t_1 \backslash t_0)] * \cdots * \underline{\underline{Q}}(t_k \backslash t_{k-1})] = \underline{\underline{PP}} \cdot [\underline{\underline{Q}}]^k \tag{3.9}$$

$$\underline{\underline{\mathbf{PP}}} = \begin{bmatrix} \leftarrow & \underline{P_A(0)} & \rightarrow \\ & \vdots & \\ \leftarrow & \underline{P_A(nN)} & \rightarrow \end{bmatrix} \tag{3.10}$$

Finally, the correlation coefficient can be found via covariance calculation [26], as stated by Equation (3.11), where $E[.]$ represents the average over the ensemble.

$$r_A(k) = \frac{E[A_o, A_k] - E[A]^2}{E[A^2] - E[A]^2} \tag{3.11}$$

3.6.2 Traffic aggregation analysis for variance-plots

It is evident that an aggregated version of $A(t)$ directly depends upon the correlation structure of its original samples. As discussed in previous Chapter, another way to see the aggregation process needed for variance-plots is as a summation of m correlated random variables, which is then multiplied by $1/m$ in order to obtain an averaged value over m samples. As a result, the analytically evaluated variance of $A[m]$, represented here by $Var(A[m]])$, is the variance of this gathering of m samples multiplied by $1/m_2$ as seen in Equation (3.12).

$$Var[A^{[m]}] = \frac{1}{m^2}\left\{\sum_{u=1}^{m}\sum_{v=1}^{m} E[A_u, A_v] - E[A]^2\right\} \tag{3.12}$$

In order to produce the variance plot required for H estimation, the variance obtained in Equation (3.12) must be normalized by the initial variance ($m = 1$). Assuming that the stochastic process is wide-sense stationary, one obtains the normalized variance, $NV(m)$, as in Equation (3.13).

$$NV(m) = \frac{Var[A^{[m]}]}{Var[A^{[1]}]} = \frac{1}{m^2}\sum_{u=1}^{m}\sum_{v=1}^{m} r_A(|u-v|) = \frac{1}{m^2}\left[m + 2\sum_{u=1}^{m-1}(m-u)r_A(u)\right] \tag{3.13}$$

Substituting the limits of correlation coefficient in Equation (3.13), it is shown in Appendix that convergence to $1/m$ and 1 happens, as it would be expected, for uncorrelated and maximally correlated traffic respectively.

3.7 Model Evaluation

Traffic features generated by the model presented above (called here basic model with hybrid forwarding) are checked against numerical simulation. In addition, complex features, which are not included in the model such as correlated forwarding, is investigated to find out how they affect the traffic features at output buffers. Comparisons are performed in a framework that is generally used to analyze self-similar traffic. This is done in order to provide a clear judgement whether traffic features are underrepresented in the analytical model studied here. An ad hoc numerical simulator generates traces with 10^5 samples for a node with 16 ports and 4 wavelengths per fiber with the purpose of validating the analytical study and providing some insight into the traffic features where analytical investigation would be rather complex. The offered load (ρ), from each 16x4 independent sources, is 0.8. A mean burst length (β) with 16 time-slots was chosen for the results presented.

3.7.1 Basic model with hybrid forwarding

For this case the offered load represented is actually 0.8/16, as seen in Equation (3.8), due to the forwarding approach utilized. The marginal distribution is shown in Figure 3.5 for both analytical and numerical models. It is also provided a Poisson density function with the same mean found in the trace. It is clear that the model generates Poisson-like densities for this node size and offered load. As expected, both methods for evaluating the marginal distribution produce the same result. This proves the number of active sources is a memoryless process.

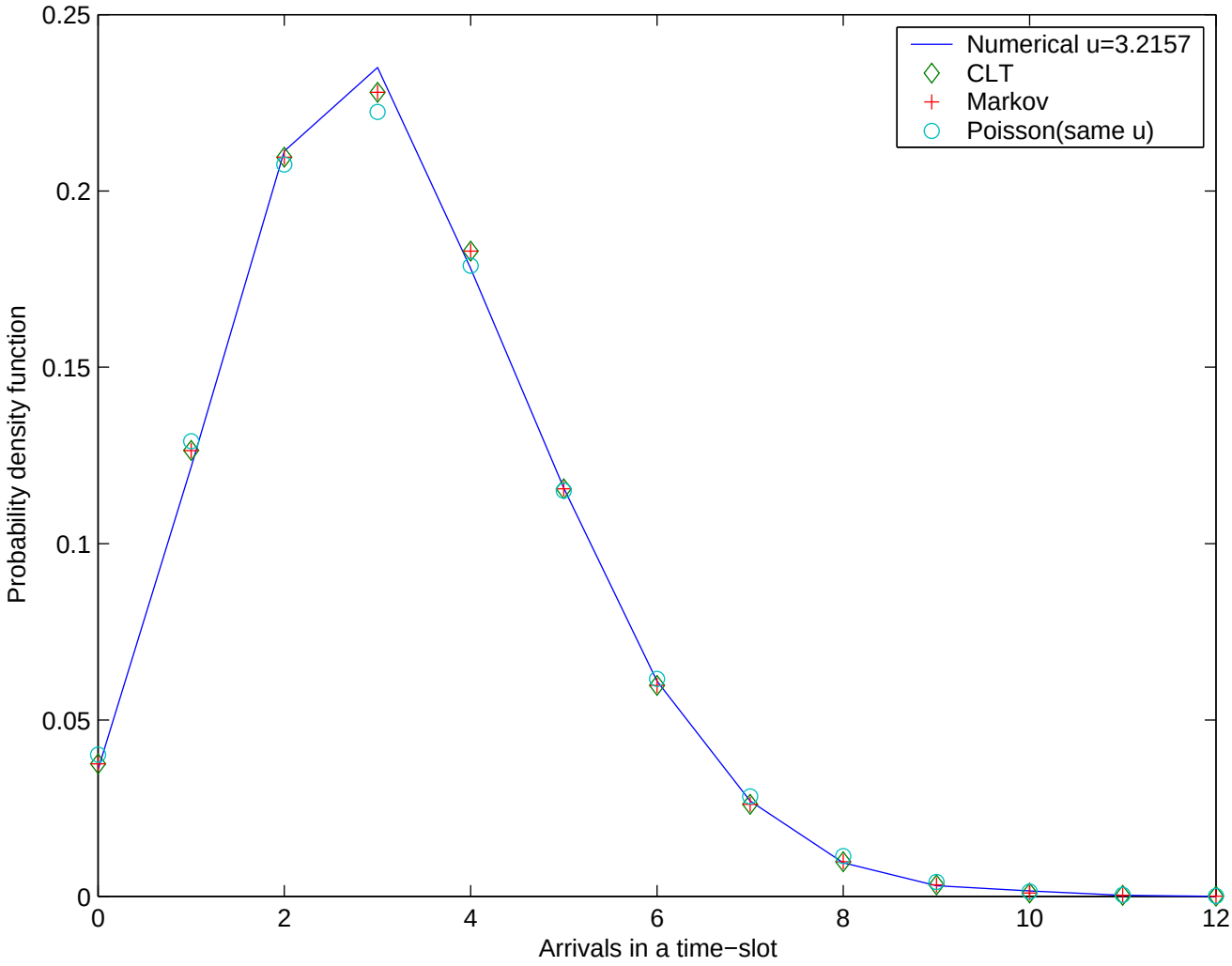

Figure 3.5: Model Evaluation: Marginal Distribution

Temporal correlation properties are exposed by autocorrelation function and aggregation analysis, shown in Figure 3.6 and 3.7 respectively. However, Figure 3.6 presents the autocorrelation obtained by the analytical procedure described in Equation (3.9) - (3.11) and numerical evaluation of traces.

It is evident the excellent agreement between them. One can observe in Figure 3.6 that the correlation is negligible for lags over 60 time-slots.

On the other hand, Figure 3.7 shows that the variance for the aggregated version of this traffic remains virtually unchanged ($H = 0.96$) until the observation period exceeds the mean burst length (16 time-slots) then a steep reduction takes place as the trace becomes practically uncorrelated after that point. This is the explanation for the good fitting to a line to $H = 0.5$ shown by trace versions with aggregation factor larger than 56 time-slots. The best fitting for the whole range studied ($m = 1000$) would produce an estimated Hurst factor $H = 0.82$. However, when the autocorrelation function is also analyzed, it is easy to conclude that this is a meaningless result

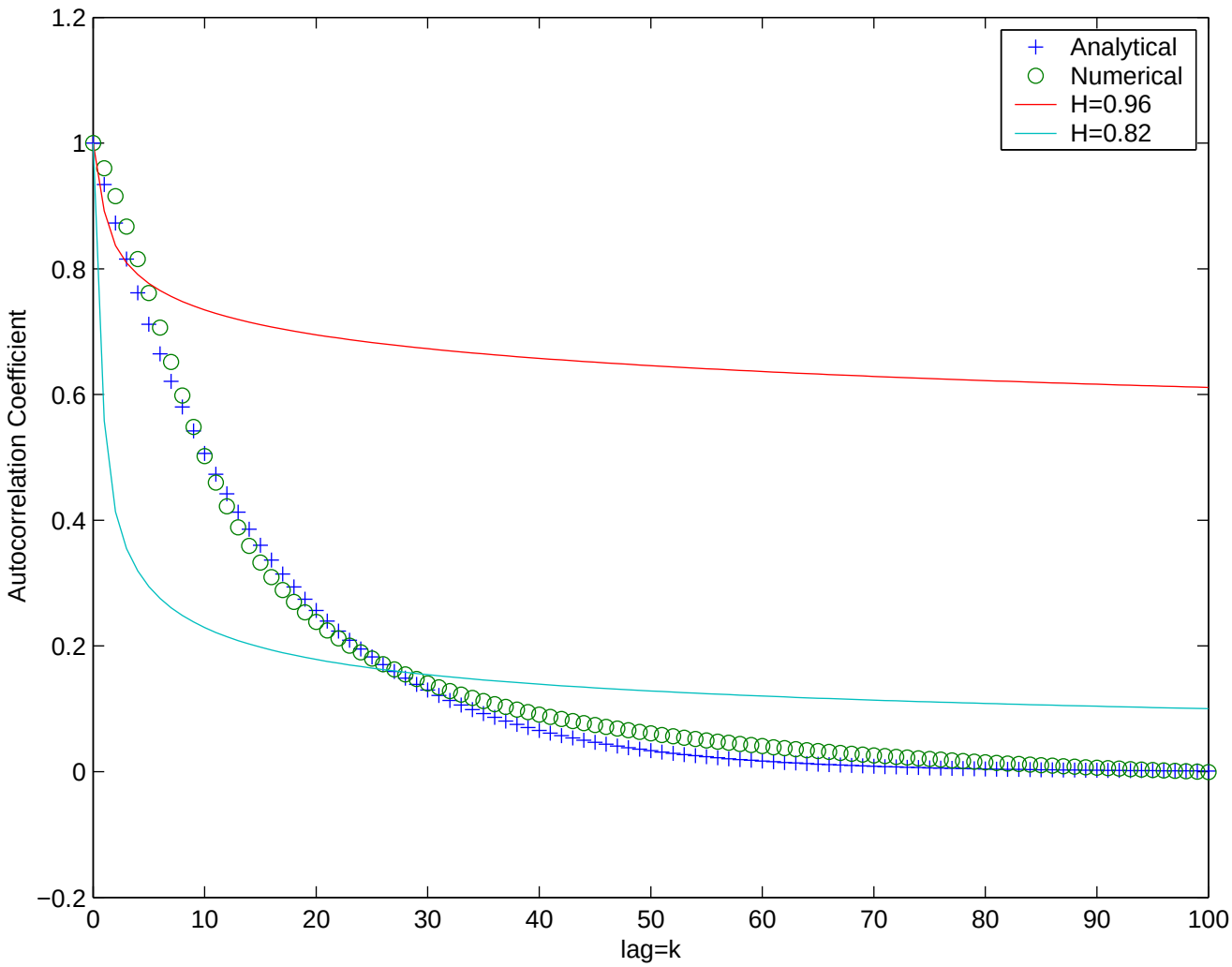

Figure 3.6: Model Evaluation: Autocorrelation

since traffic correlation present in this trace is short-range only. Nonetheless, it must be said that the trace has stronger correlation properties than an equivalent self-similar trace with $H = 0.82$ for lags below 29 time-slots.

3.7.2 Strictly correlated forwarding

If it is considered strictly correlated forwarding, the whole burst is always headed for a given outlet. For this reason it is required to perform *"Traffic Shaping"*. The way packets are assigned to allocated time-slots influences the correlation structure of the traffic. One may assign the payloads in a sequential and deterministic form within the number of time-slots allocated for each aggregate as in Figure 3.8.

On the other hand, an alternative way would involve a random assignment instead, as shown in Figure 3.9.

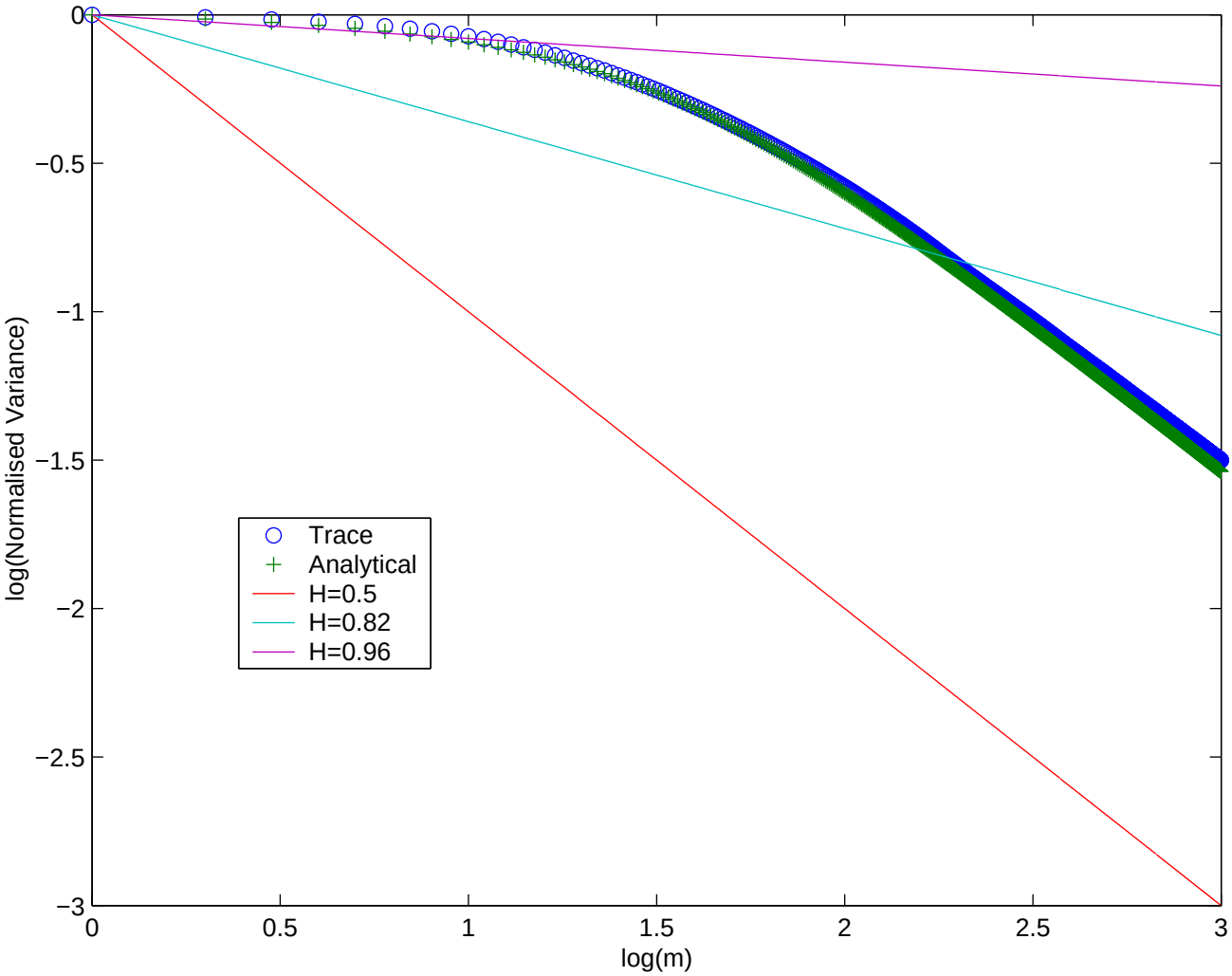

Figure 3.7: Model Evaluation: Variance-plot

However, this sequential assignment is not a wide sense stationary process since the time invariance for the autocorrelation does not hold for this case. Instead this process is a cycle-stationary stochastic process since it arises from the repetition of a stationary process at every aggregate size time-slots. Alternatively, one should look at this process through an averaged version of correlation coefficient function. The sequential assignment provides bursts generation for strictly correlated forwarding. A sequential placement of packets in time causes no penalty to (mean) node performance provided that, on average, the load is well distributed amongst wavelengths. With respect to the autocorrelation coefficient for sequential allocation, the deterministic placement of packets at the begging of each group of time-slots produces periodic peaks nN lags apart (the width of peaks indicates the range of dependance); on the other hand, the lack of packets at the end of nN time-slots gives rise to the negative correlation; an averaged version of this autocorrelation is the one expected by analytical methods, this autocorrelation coefficient is shown in Figure 3.10 and the variance is also shown in Figure 3.11 where the convergence to $H = 0.5$ is reached when increasing

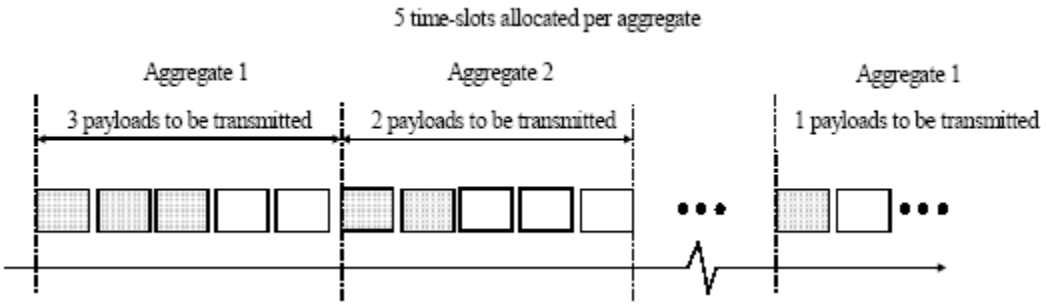

Figure 3.8: Traffic shaping: Sequential

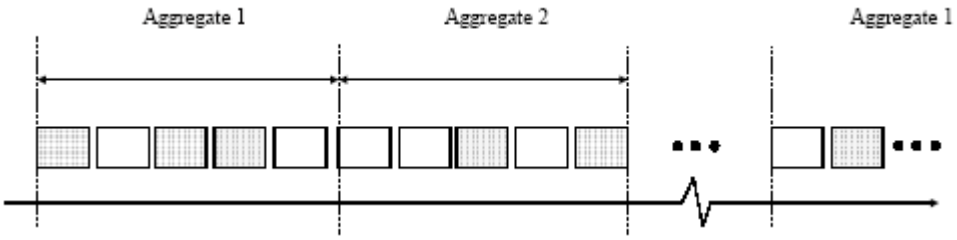

Figure 3.9: Traffic shaping: Random

the aggregation factor m.

When packets are allocated randomly across the time-slots, no correlation is present in the traffic and the variance of the aggregated process is always similar to $H = 0.5$ as shown in Figure 3.12 and Figure 3.13.

As far as statistical traffic features are concerned, no significant difference is noticed between the hybrid model and the strictly correlated forwarding by sequential assignment taking into account marginal densities, aggregation and autocorrelation functions.

3.8 Discussion

Once the model under analysis has proved to be accurate enough in representing important traffic features, issues related to performance assessment are now briefly discussed, allowing some important conclusion to be drawn regarding node performance evaluation.

3.8.1 Correlation span and performance

Before assessing buffer performance, one should carefully examine the traffic features reaching the buffer in order to better interpret outcomes of such experiments. The results presented in Figure 3.14 are for summation of the correlation coefficients (from lags 1 to 100) against node size for different burstiness and offered load. This procedure is used here to obtain concise results regarding correlation behavior against all variables of the problem under analysis. A clear indication, provided by Figure 3.14, is that little difference is to be expected from assessments of nodes size over 16

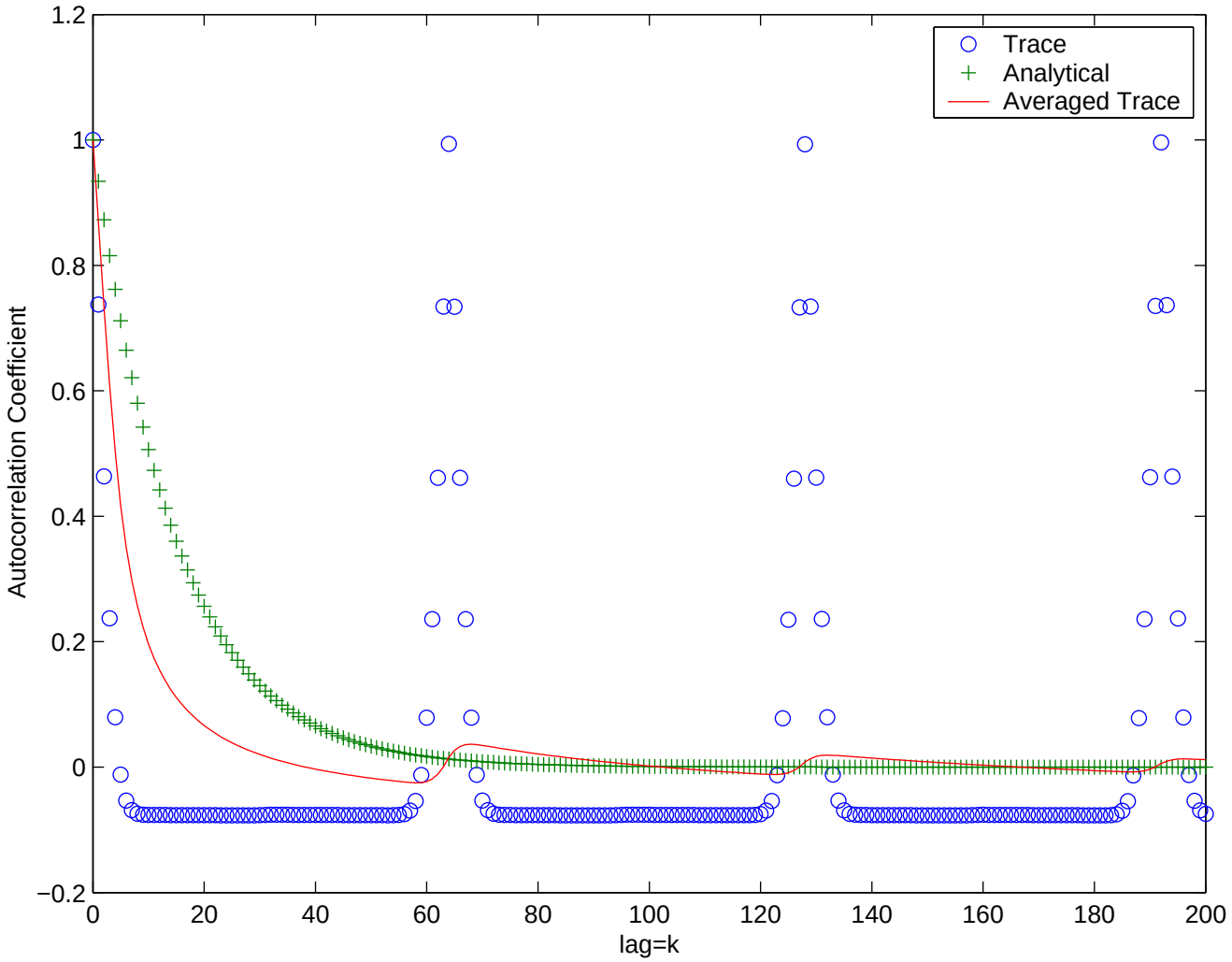

Figure 3.10: Autocorrelation by sequential assignment

ports, as far as influence of correlation on performance is concerned. Lower levels of traffic produce higher levels of correlation. Less sensitive is the correlation to changes of node size for the case of low offered load. The higher the burstiness the wider the difference between curves for low and high offered load.

Although it is clear that this traffic model only produces SRD, the correlation length is unbounded as Figure 3.14 demonstrates when β is increased. Therefore, the inclusion of long-range dependence may only have minor importance in the context of the present study. More evidences to support this argument can be found in [21] and [40]. Moreover, the levels of short-range dependence match (or even exceed) the correlation levels from exact self-similar traffic within the range that might be realized by the optical buffer, as shown in Figure 3.6 and 3.7.

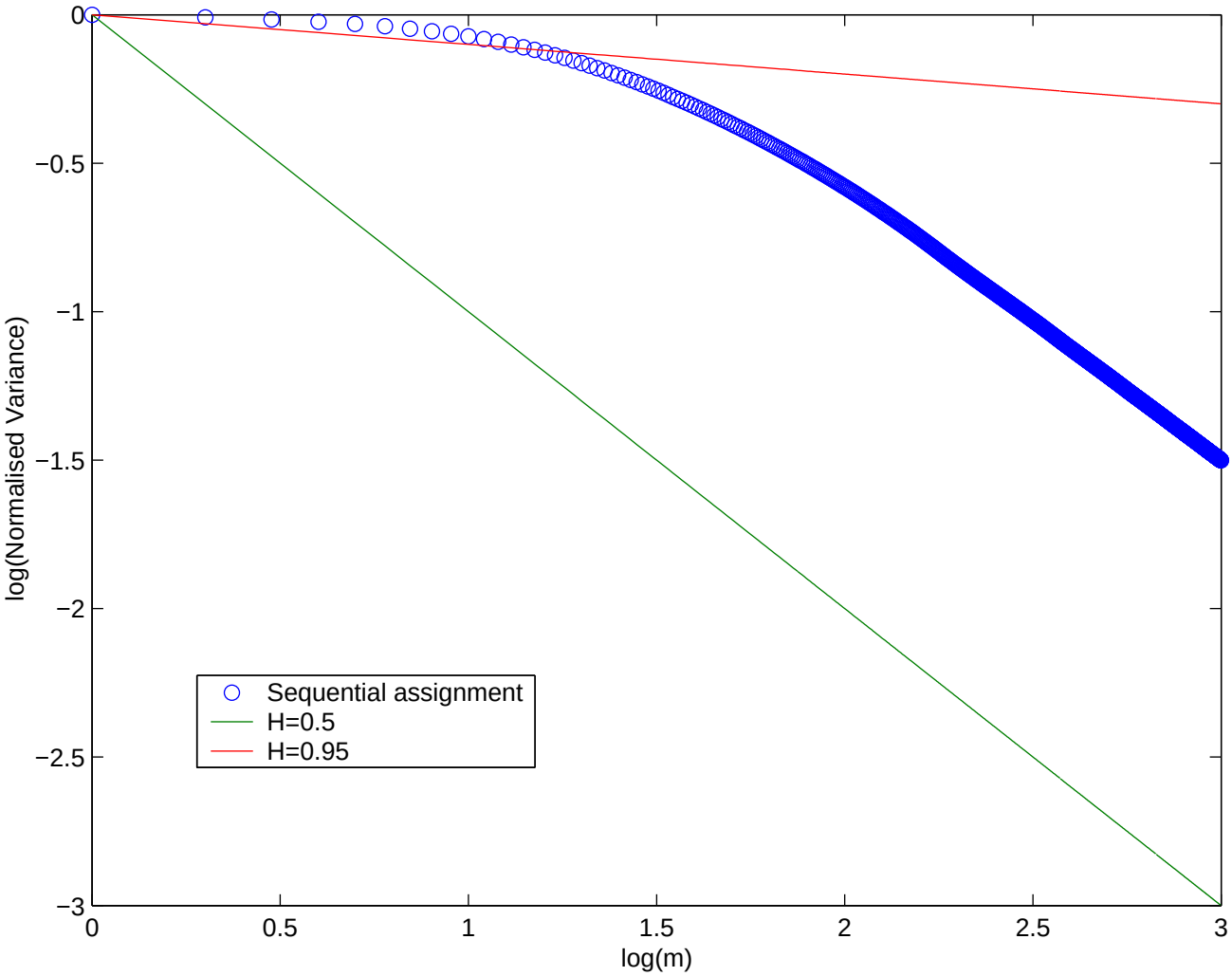

Figure 3.11: Variance by sequential assignment

3.8.2 Marginal distribution and performance

The marginal distribution for the model under analysis is expected to converge to a Poisson like distribution (which converges to Gaussian for large means). The convergence of distributions is generally studied via Quantile-Quantile plots [33] or simply displaying the cumulative distributions together. Nevertheless, these charts only provide a qualitative, and therefore subjective, appreciation of the convergence. A simple summation of squared difference is proposed in Equation (3.14) for comparing the analytical evaluated marginal distribution and a Poisson probability density function using the same mean.

$$\Delta_{Poisson} = \sum_i [pdf\_model(i) - pdf\_Poisson(i)]^2 \tag{3.14}$$

The results presented in Figure 3.15 show the well-known convergence to a Poisson density when the node size is increased. The more wavelengths are in use the faster is this convergence.

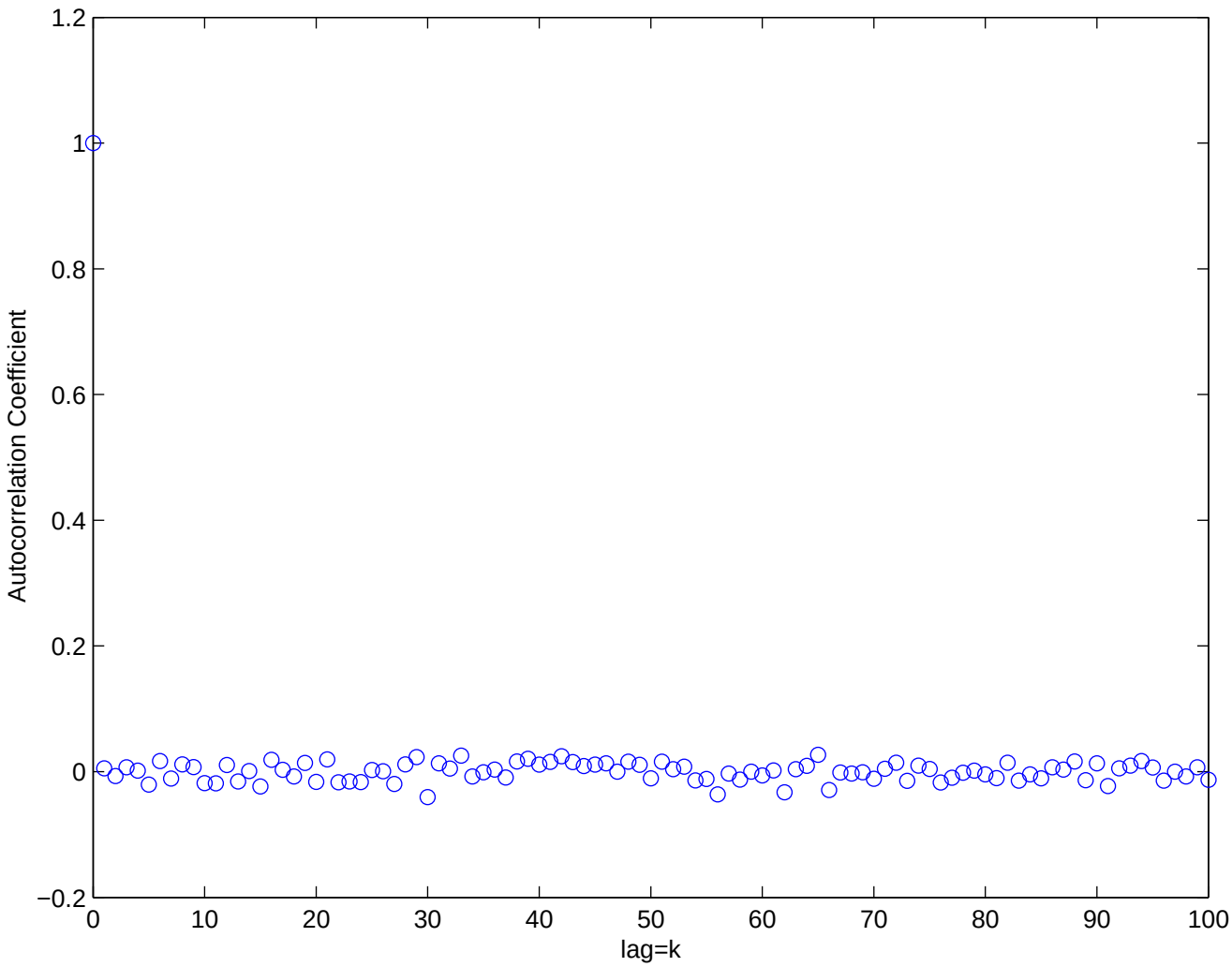

Figure 3.12: Autocorrelation by random assignment

This result is, however, insensitive to burstiness variations. For nodes larger than 8x8 the marginal density quickly converges to Poisson regardless of number of wavelengths. Although the results presented in Figure 3.15 is only for $\rho = 0.8$, the lower the offered load the faster is this convergence.

In summary, results from performance evaluation for nodes more than 16x16 ports with a given buffer depth are expected not to vary much (for a given burstiness) since both correlation structure and marginal distribution remain practically unchanged for such node size.

3.9 Performance assessment for buffering

The traffic produced by the model under analysis is now used to evaluate the effectiveness of buffering in reducing contention in photonic switching. Although most of the results shown in this

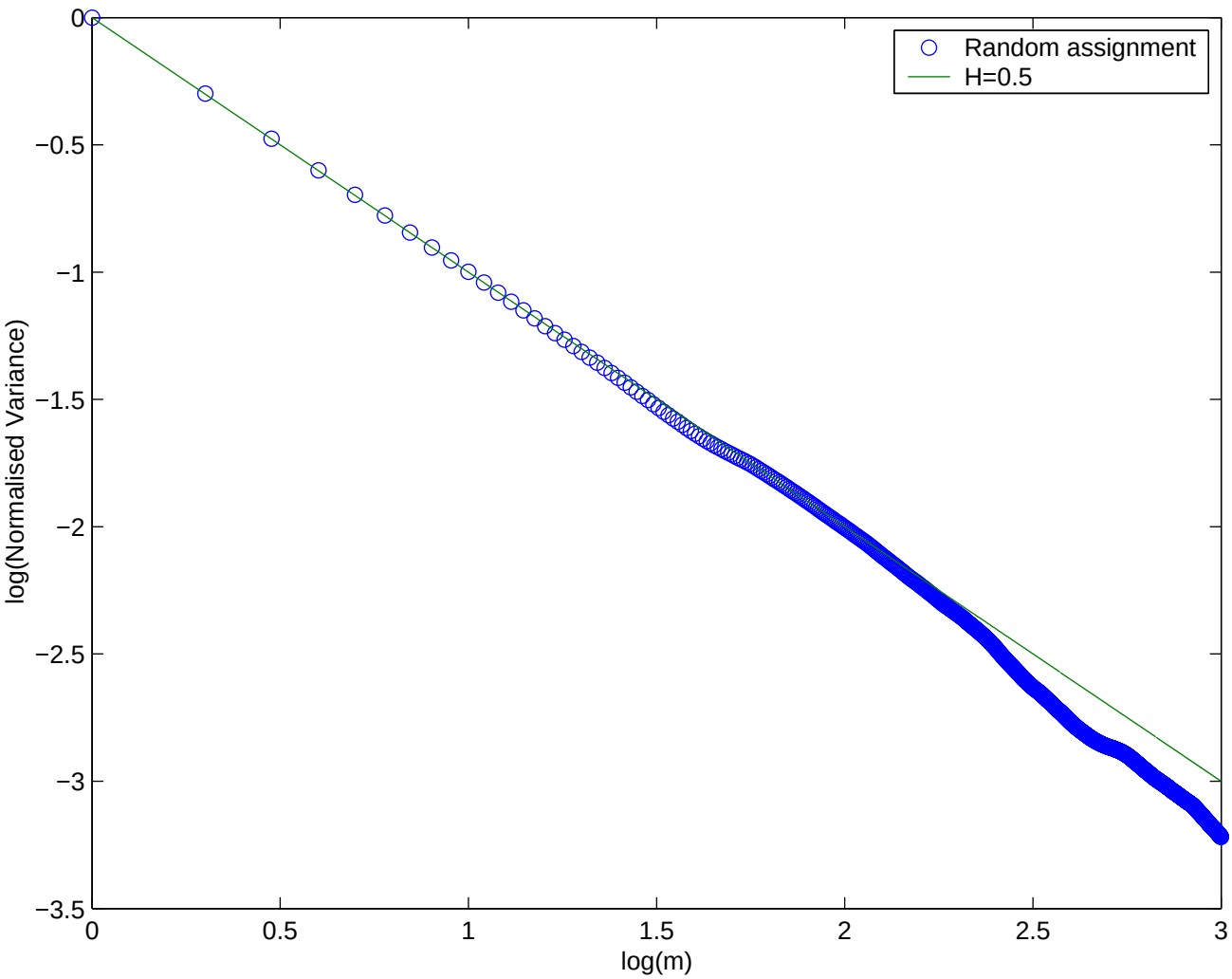

Figure 3.13: Variance by random assignment

section are already known, a contribution is made toward an exact method to evaluate performance of WDM nodes under correlated traffic.

3.9.1 Bufferless nodes

The first architecture to be evaluated actually possesses no buffer. This fact provides an interesting reference for further comparisons since performance is only dependent on features associated to the marginal distribution. The system is unable to realize any temporal correlation due to the lack of memory of past events. In order to deal with contending packets, only WDM and TWC can be used, and, as a result, the switch packet loss probability (PLP) calculation is straightforward in Equation (3.15). Arrivals headed for a given output that exceed the number of wavelengths available are simply lost. This is traduced by the tail integration of $p_A(a)$.

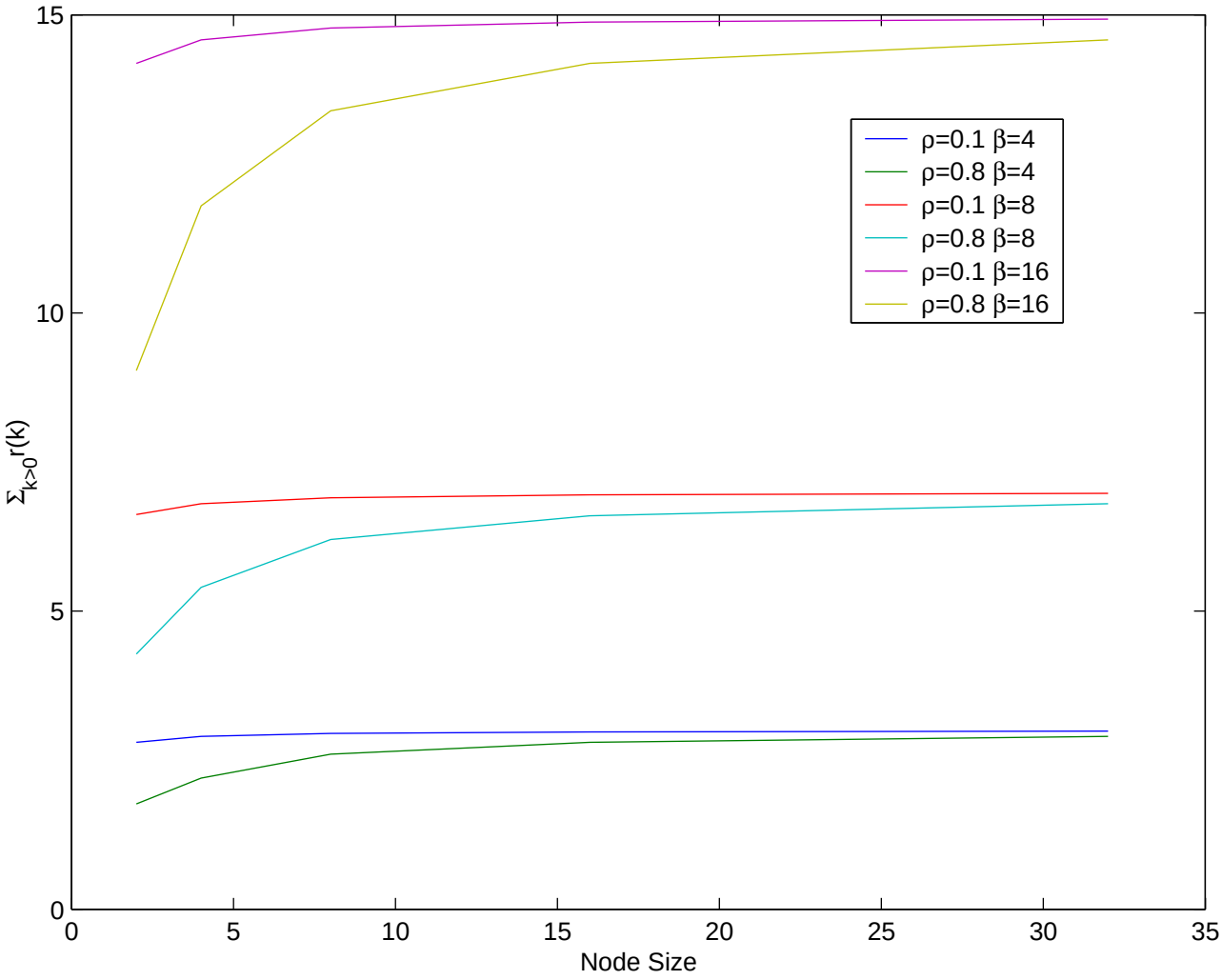

Figure 3.14: Summation over 100 time-slots for correlation coefficient

$$PLP = \frac{1}{n\rho}\int_{a>n}^{\infty} P_A(a)da = \frac{1}{n\rho}\sum_{j=n+1}^{nN} P_A(j) \tag{3.15}$$

Whenever contention takes place, wavelength conversion makes possible the use of another wavelength for transmitting contending packets unless all wavelengths are already taken. It is easy to foresee that performance of bufferless nodes will not reach satisfactory levels unless the load per wavelength is very low. In Figure 3.16 performance evaluation is shown, along with numerical validation, considering nodes operating under both shared and non-shared load regimen. For the former each wavelength added to the system takes a share of the load transported (ρ/nN), while latter maintains individual loads (ρ/N) unaffected after inclusion wavelengths. As a result, negligible improvements are found for unshared regimen. Little sensitivity is observed for both load regimes regarding node sizes due to convergence of the marginal distribution as discussed previously.

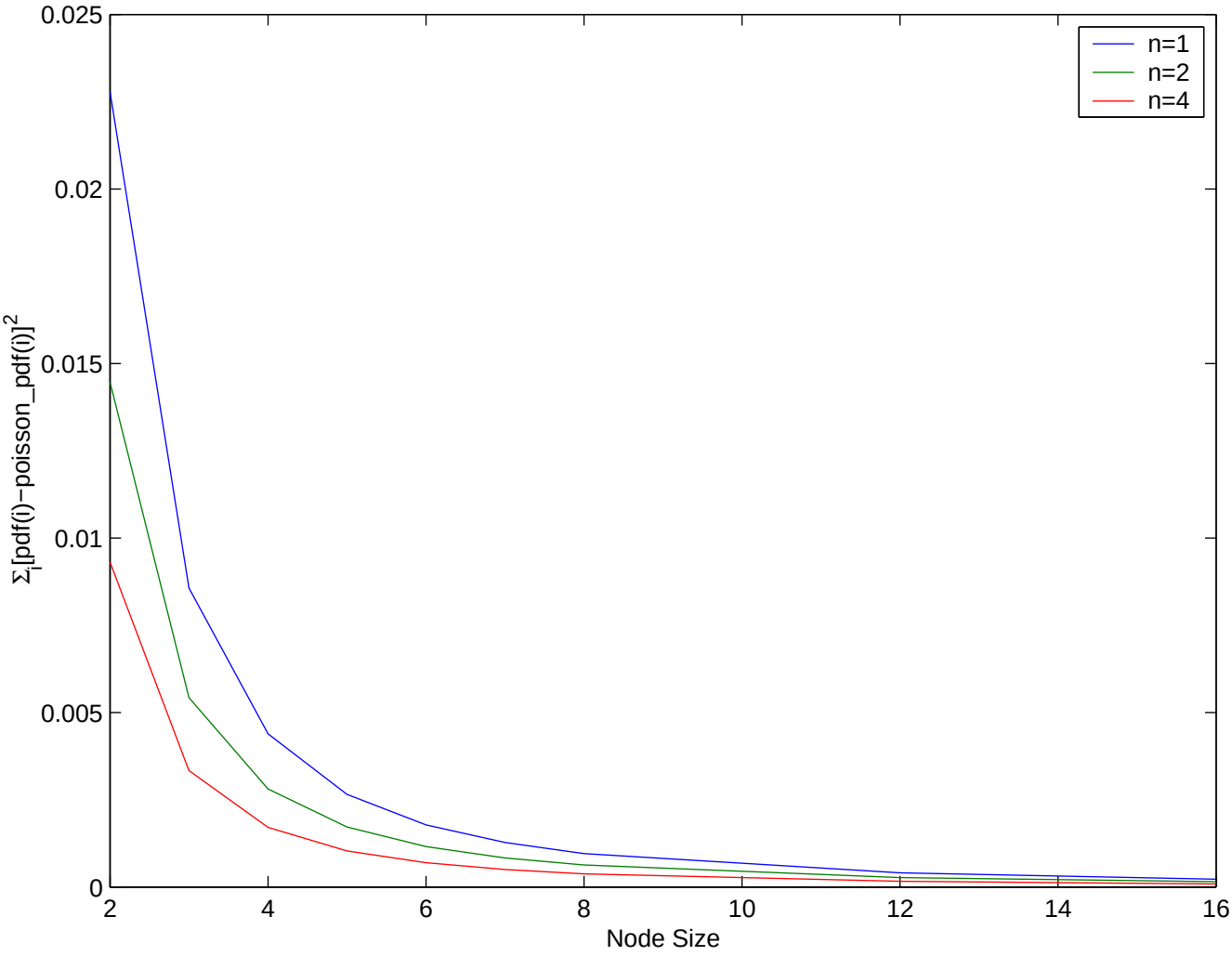

Figure 3.15: Comparison: marginal with Poisson distribution for $\rho = 0.8$

However, as expected, better results are obtained for shared load regimen. By using 11 wavelengths one can have nodes with PLP lower than 10^{-10}. Although results concerning packet loss probability are very encouraging, overall throughput for load-shared architecture is expected to be very low since the traffic transported by wavelength must be low. The purpose of including buffering is to add one more degree of freedom in managing contention, improving performance for unshared load and keeping node total throughput high.

3.9.2 Buffer performance under uncorrelated traffic

The number of fiber-delays at each output is represented by b, as shown in Figure 3.1. However, the actual storage capacity of this set of fiber-delays can be improved if one considers that n packets can occupy each physical position in this buffering system simultaneously. This is possible due to the use of wavelength conversion and WDM bringing the storage capacity up to $B = nb$. The stochastic

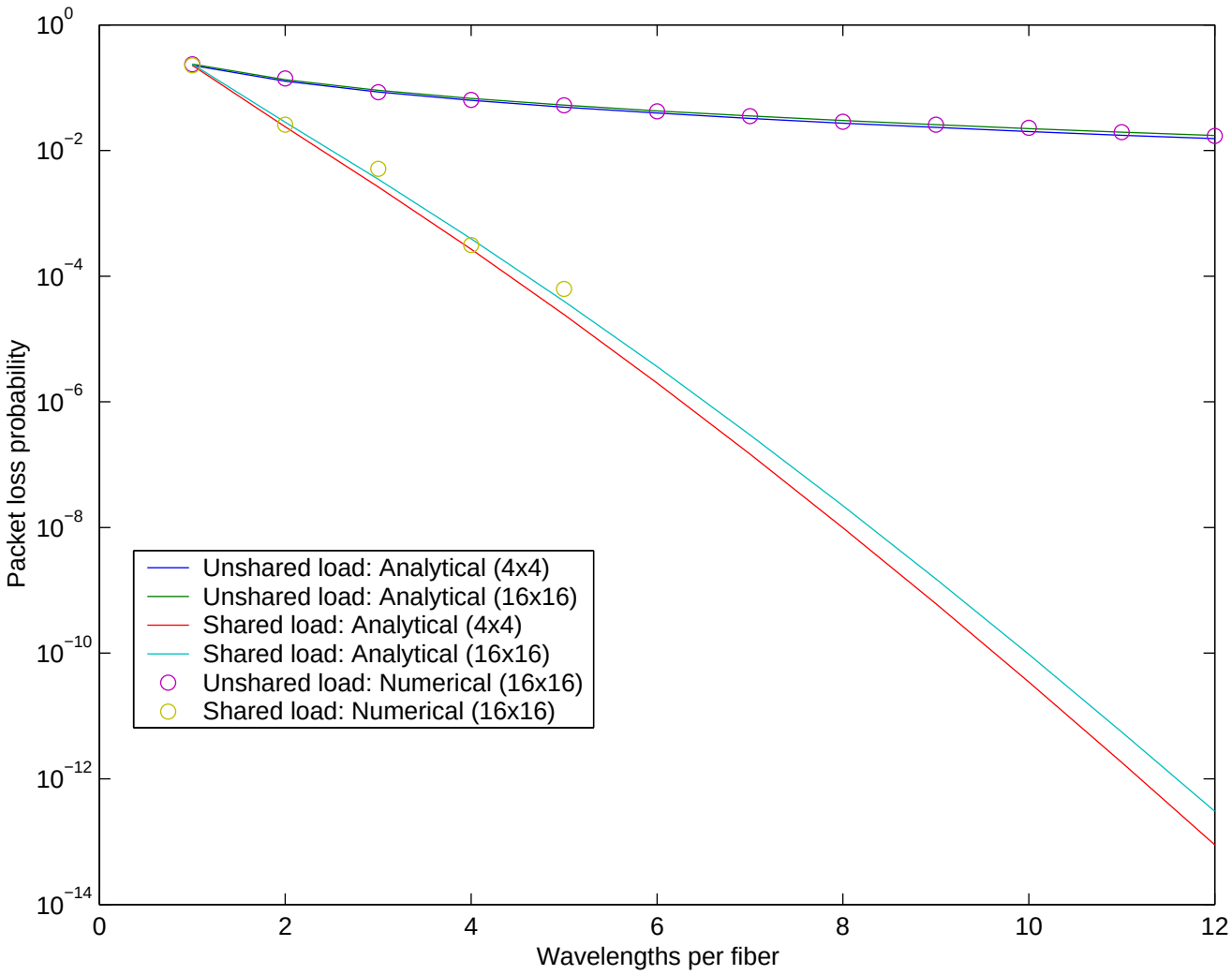

Figure 3.16: Performance Evaluation for bufferless nodes $\rho = 0.8$

process representing temporal evolution of buffer occupancy is specified from the stochastic process for packet arrival $A(t)$ arrival, buffer depth B, and number of wavelengths n serving the queue system. Where $min\{u, v\}$and $max\{u, v\}$ stand for the minimum and maximum functions between u and v respectively as shown

$$\Theta(T) = min\{max\{[\Theta(T-1) + A(T) - n], 0\}, B\} \tag{3.16}$$

A given temporal sample of this process is evidently confined between 0 and B. The marginal distribution for this random variable is $p_\Theta(\theta) = Prob[\Theta = \theta]$ with $\theta \in \{0, 1, 2, ..., B\}$. For the sake of convenience, this probability density function is represented q in a vector form, i.e. $q = [q_0 = p_\Theta(0)...q_B = p_\Theta(B)]$. A Markov chain representing Equation (3.16) would have its boundaries (given by max and min functions) as in Figure 3.17.

Therefore, from Equation (3.16) the transition probability between states [10], [18], represented

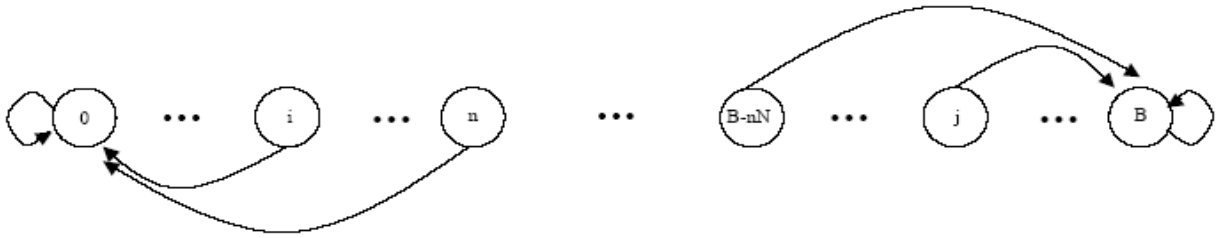

Figure 3.17: Illustration for the boundaries for the Markov chain used to represent buffer state.

by P_{ij}, for this Markov chain is given in Equation (3.17) where i is the state at T and j is the state at $T+1$,

$$P_{ij} = Prob[\Theta(T+1) = j | \Theta(T) = i] = \begin{cases} \sum_{l=0}^{n-i} P_A(l) & 0 \leq i \leq n, j = 0 \\ P_A(j-i+n) & 0 \leq i \leq n, 1 \leq \text{j} \leq B-1 \\ P_A(j-i+n) & n+1 \leq i \leq B, i-n \leq \text{j} \leq B-1 \\ \sum_{l=B-i+n}^{nN} P_A(l) & 0 \leq i \leq B, j = B \\ 0 & \text{otherwise} \end{cases} \tag{3.17}$$

The steady-state solution of the Markov chain is found by solving the Equation system presented as follows, where e is a unitary row vector with $B+1$ elements

$$\begin{cases} \underline{q} = \underline{q} * \underline{\underline{P}} \\ \underline{q} * \underline{e} = 1 \end{cases} \tag{3.18}$$

For a specific outlet the average number of packets that leave the queue in a time-slot is denoted, $1 - \rho_{0\lambda}$, where $\rho_{0\lambda}$ is the mean number of packets that are not used [10] at the given outlet. The mean number of packets that arrive at the queue in each time-slot is found to be, ρ. We are now able to determine the switch packet success probability, $PSP = 1 - PLP$ (PLP is the switch packet loss probability), which is the number of successfully transmitted packets, $1 - \rho_{0\lambda}$, divided by the mean number of packets that enter the queue in each time slot, ρ. From the distribution of packets in the queue the mean number of unused wavelengths can be calculated as

$$\rho_{0\lambda} = \sum_{i=0}^{n} \sum_{j=0}^{n-i} P_A(j) q_i \cdot [n - (i+j)] \tag{3.19}$$

Finally we can write the switch packet loss probability (PLP) as

$$PLP = 1 - PSP = 1 - \frac{n - \rho_{0\lambda}}{n\rho} \tag{3.20}$$

where PSP is the Packet Success Probability.

The model presented above actually is a queuing system with n servers (G/D/n/nb). The exploitation of the wavelength domain is now analyzed.

Multiple server and buffer depth multiplication

In order to find out the effect of multiple server and delay sharing, here is shown Figure 3.18.

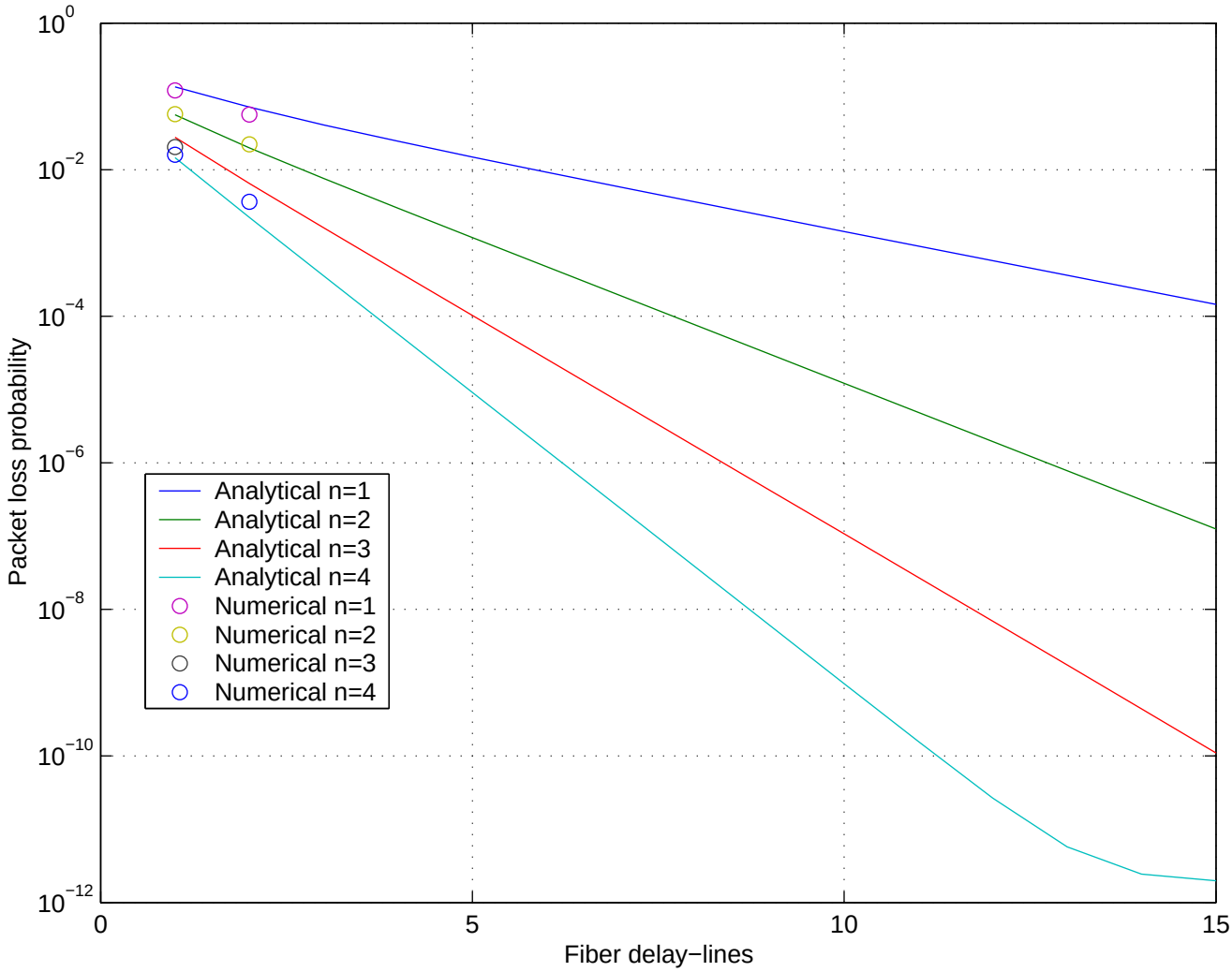

Figure 3.18: Packet Loss Probability versus number of fiber-delays (buffers) for nodes using WDM

It can be seen good results when delay sharing by WDM is implemented [10]. Using ten fiber-delays and $n = 4$, for example, the packet loss probability is decreased by 6 orders of magnitude, as can be seen in Figure 3.18. This is because the traffic load to the tagged output is also increased when n grows but no significant change is noticed for the marginal distribution. As a result, more wavelengths allow more packets to share the same fiber-delay benefiting the total buffer depth.

Buffer depth requirements for a performance target

The evaluation of buffer depth reduction (for $PLP < 10^{-10}$) versus number wavelength channels for light and heavy load per wavelength are presented in Figure 3.19 and 3.20 respectively. As it might be expected, the required buffer depth for a given PLP approximately decreases at $1/n$, due to the multiplication by n of buffer positions. As anticipated, no significant change in performance is noticed for nodes larger than 16x16.

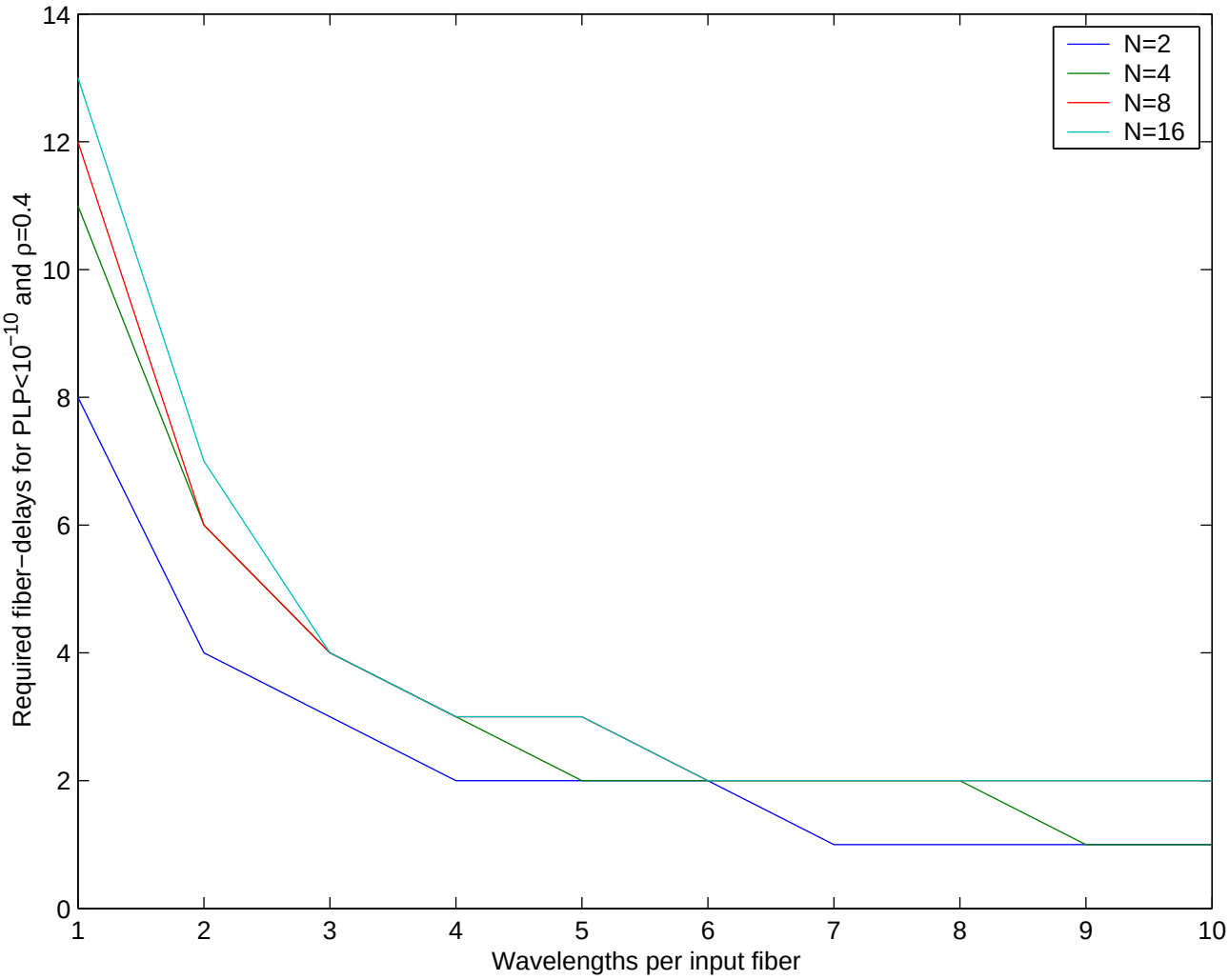

Figure 3.19: Required buffer depth, for packet loss probability less than 10^{-10}, versus number of wavelength per fiber: $\rho = 0.4$

Another feature not seen before, will be shown below. The evaluation of buffer depth (for $PLP < 10^{-10}$) versus load is presented in Fig. 3.21 for one channel per fiber.

It can be seen that no significant change in performance is noticed for nodes larger than 16x16. The greater the load, the greater the buffer depth; the greater N, the greater the buffer depth. A buffer size of 17 delay-lines will carry a load of 0.5 for support a packet loss probability less than

10^{-10} for 16 fibers.

3.9.3 Buffer performance under time-correlated traffic

The results presented so far for buffered nodes under uncorrelated traffic provide performance upper bounds for switching node performance since no temporal dependence is present in the traffic correlation structure. As a result, the sequential placement of packets has to be used at the expense of creating time correlation and, as far as buffering is concerned, creating a more demanding traffic profile. Here we focus on a shared buffer.

Some alterations are necessary in the model previously discussed in order to allow it to take into account time-correlation. The Markov chain representing the buffer state, in this case, should also hold the number of inputs in High state [3], comprising therefore $(nN+1)$ x $(B+1)$ elements as the vector holding the probability density for buffer occupancy as given in

$$\begin{array}{ccccc} \sum_{i=0}^{nN} q_{0i} = q_0 & & & & \sum_{i=0}^{nN} q_{Bi} = q_B \\ q = [\overbrace{q_{00} \cdots q_{0nN}} & \cdots & \cdots & & \overbrace{q_{B0} \cdots q_{BnN}}] \end{array} \tag{3.21}$$

The transition matrix between buffers states, now represented by $\underline{\underline{\Pi}}$, still has $(B+1)$ x $(B+1)$ elements as shown in

$$\underline{\underline{\mathbf{\Pi}}} = \begin{bmatrix} \underline{\underline{\pi_{0,0}}} & \cdots & \underline{\underline{\pi_{0,B}}} \\ \vdots & \ddots & \vdots \\ \underline{\underline{\pi_{B,0}}} & \cdots & \underline{\underline{\pi_{B,B}}} \end{bmatrix} \tag{3.22}$$

However, each element of this matrix is itself a sub-matrix with $(nN+1)$ x $(nN+1)$ components [3]. This sub-matrix takes into account the transition among source states, as it can be seen in

$$\pi_{\mathbf{i,j}} = \begin{bmatrix} P_{ij}^{\{0\}} Q_{0,0} & \cdots & P_{ij}^{\{0\}} Q_{0,nN} \\ \vdots & \ddots & \vdots \\ P_{ij}^{\{nN\}} Q_{nN,0} & \cdots & P_{ij}^{\{nN\}} Q_{nN,nN} \end{bmatrix} \tag{3.23}$$

where Q_{mw} is the transition probability from m to w for the number of sources at ON state producing packets, and is given by

$$Q_{mw} = \sum_{i=0}^{nN-m} \sum_{j=0}^{nN} T_m(i) S_m(j) \delta_{w,m-j+i} = \begin{cases} \sum_{j=m-w}^{min(m,nN-w)} T_m(w-m+j) S_m(j) & \text{, if } m >= w \\ \sum_{i=w-m}^{min(w,nN-m)} T_m(i) S_m(m-w+i) & \text{, if } m <= w \end{cases} \tag{3.24}$$

where $T_m(i)$ (or $S_m(j)$) represents the probability that i (or j) sources pass from the OFF state to the ON state (or viceversa), given that m of them are in ON state. Hence, we can see

$$\begin{array}{l} T_m(i) = \binom{nN-m}{i} R_{LH}^i (1-R_{LH})^{nN-m-i} \\ S_m(j) = \binom{m}{j} R_{HL}^j (1-R_{HL})^{m-j} \end{array} \quad (3.25)$$

Notice that $P_{i,j}^{\{c\}} = Prob[\Theta(T) = j | \Theta(T-1) = i, C = c]$ is the same transition probabilities shown in Equation (3.17) but the number of sources in High state conditions the arrival probability. For the particular case of on-off sources, the probability of having i arrivals when c sources addressed to the tagged output are in High state can be straightforwardly represented as given next, since as the amount of packets released is deterministic once the number of active sources is set.

$$P_A^{\{c\}}(a) = P_A(a|c) = \binom{c}{a} \mu_H^a (1-\mu_H)^{c-a}; \text{ for } \mu_H = 1 \text{ we have: } P_A^{\{c\}}(a) = \binom{c}{a} 0^{c-a} = \delta_{a,c} \quad (3.26)$$

The steady state solution for buffer occupancy is found solving the next Equation system where e is again a unitary column vector but in this case with $(nN+1)$ x $(B+1)$ elements

$$\begin{cases} \underline{q} = \underline{q} * \underline{\underline{\Pi}} \\ \underline{q} * \underline{e} = 1 \end{cases} \quad (3.27)$$

Once q is found, the source states must be collapsed, as shown in Equation (3.21), and therefore Equation (3.19) - (3.20) can be applied in order to work out the packet loss probability for correlated traffic, i.e. $\rho_{0\lambda}$ is given by

$$\rho_{0\lambda} = \sum_{i=0}^{n} \sum_{j=0}^{n-i} \sum_{k=0}^{nN} p_A^{\{k\}}(j) q_{ik}(n-(i+j)) \quad (3.28)$$

Burstiness intensity and buffer depth

Results in Figure 3.22 and 3.23 investigate the influence of burstiness on efficiency of buffers in reducing packet loss probability for light and heavy traffic loads, respectively.

It is clear the performance degradation due to the presence of time-correlation among arrivals. The slow decrease of packet loss versus buffer depth shows that even large buffers are not able to take the performance to reasonable values as temporal correlation increases. It can be seen that the offered load has little effect when the burstiness factor is high.

Node size and buffer depth

The effect of the switch size and the buffer performance for two values of burstiness is shown in Figure 3.24 and 3.25.

The larger is the switch the worse is the performance. But no major change is noticed for nodes larger than 16x16, alike the uncorrelated case, except when burstiness is changed. Recall that in this case both marginal distribution and correlation structure influence performance. Node size shapes both correlation (via Low period -see Equation (3.3)) and marginal distribution as seen in

Figure 3.14 and Figure 3.15. Regardless to the fact that for large node sizes no change is noticed in the correlation span, the High period (β) still affects the length of correlation and, therefore, buffering performance.

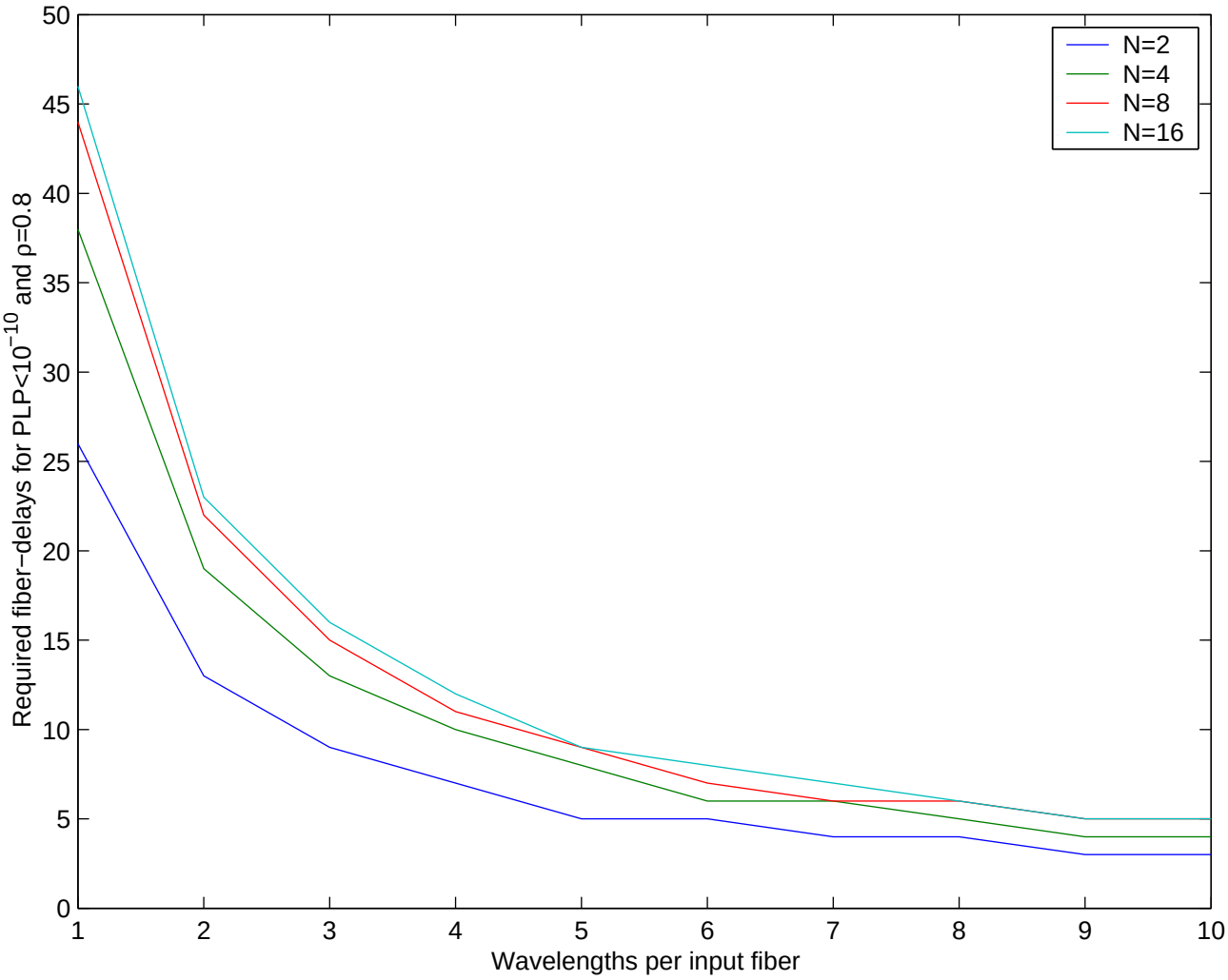

Figure 3.20: Required buffer depth, for packet loss probability less than 10^{-10}, versus number of wavelength per fiber: $\rho = 0.8$

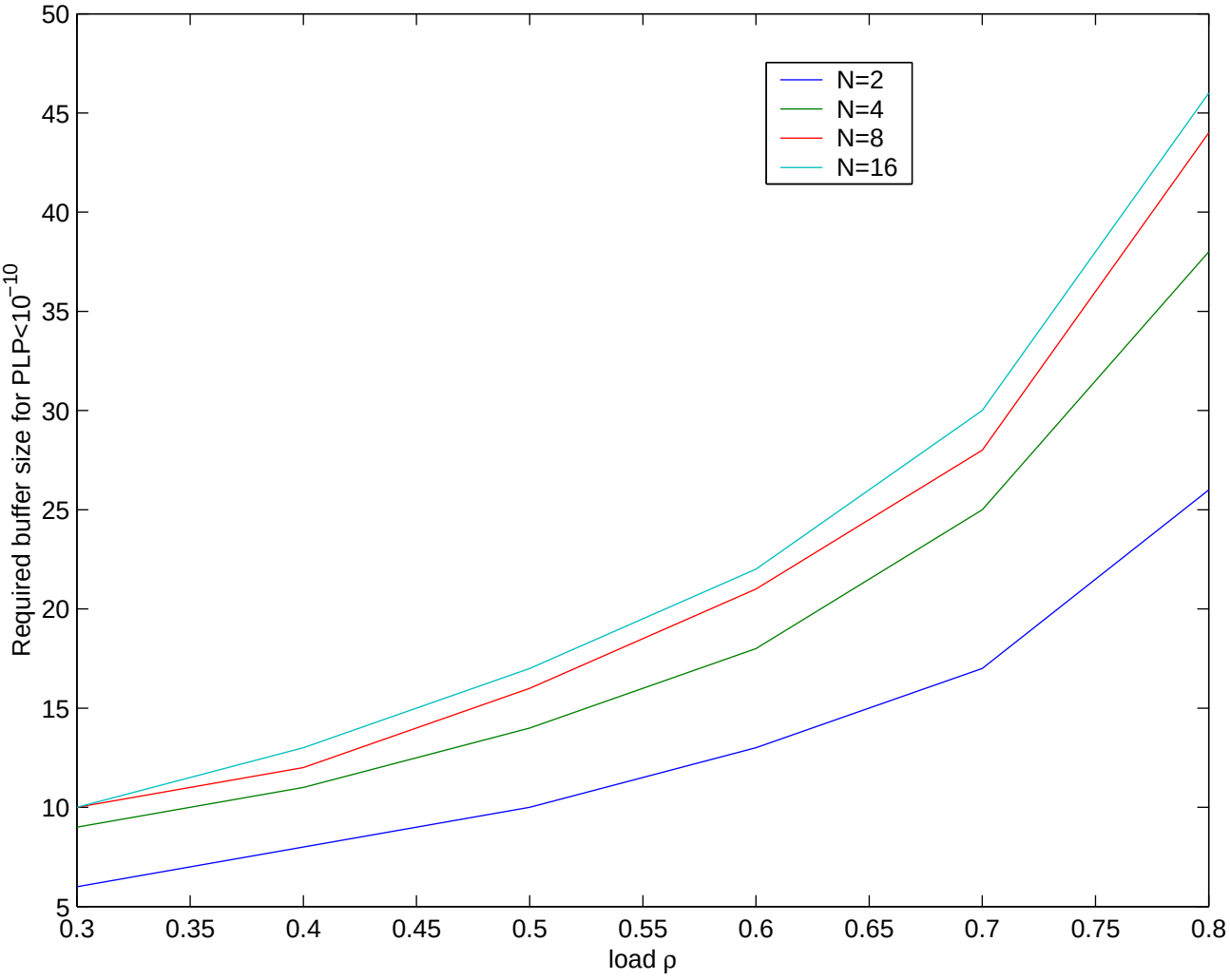

Figure 3.21: Required buffer depth, for packet loss ratio less than 10^{-10} versus load.

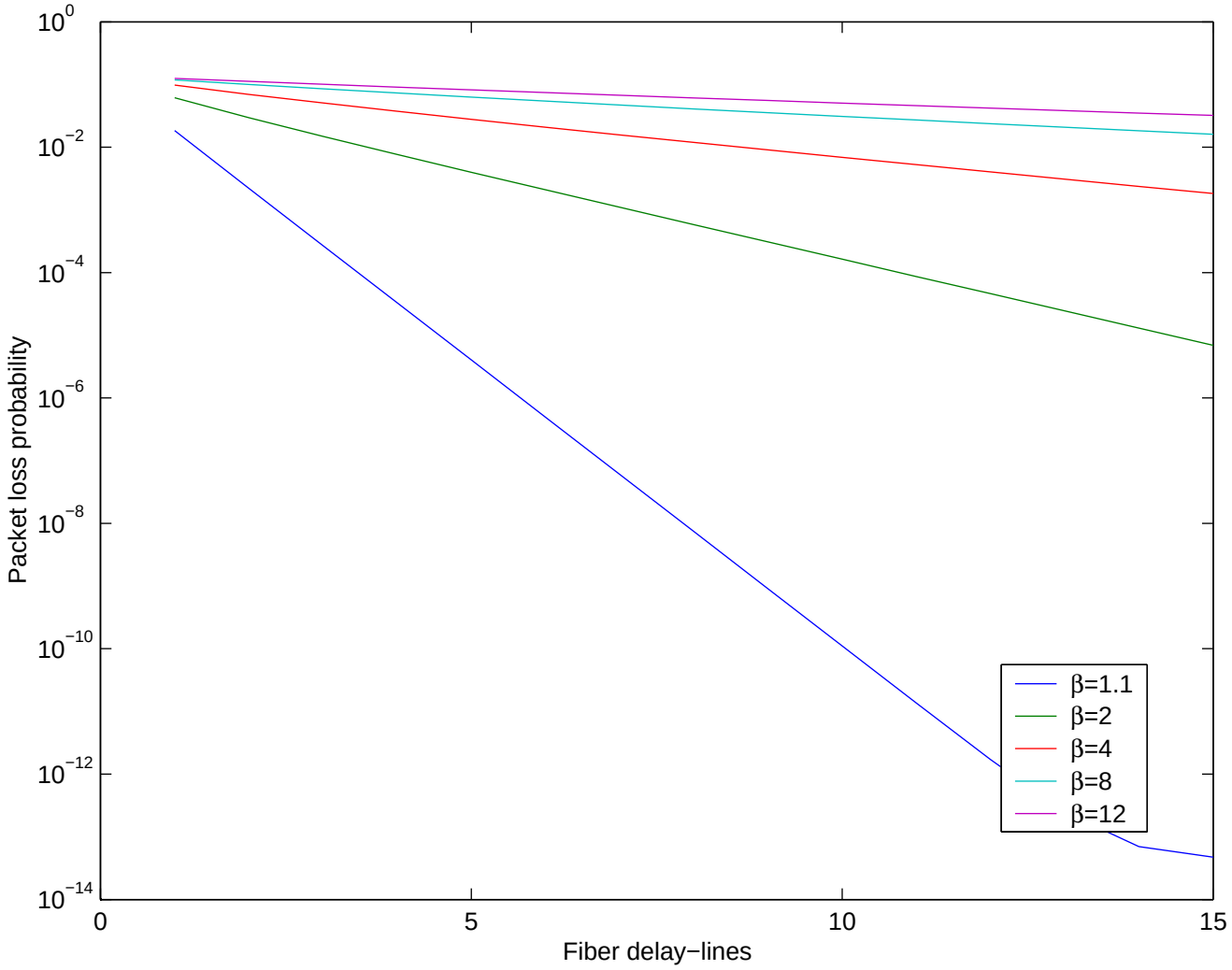

Figure 3.22: Packet Loss Probability versus buffer depth using burstiness as a variable parameter: load per channel 0.4

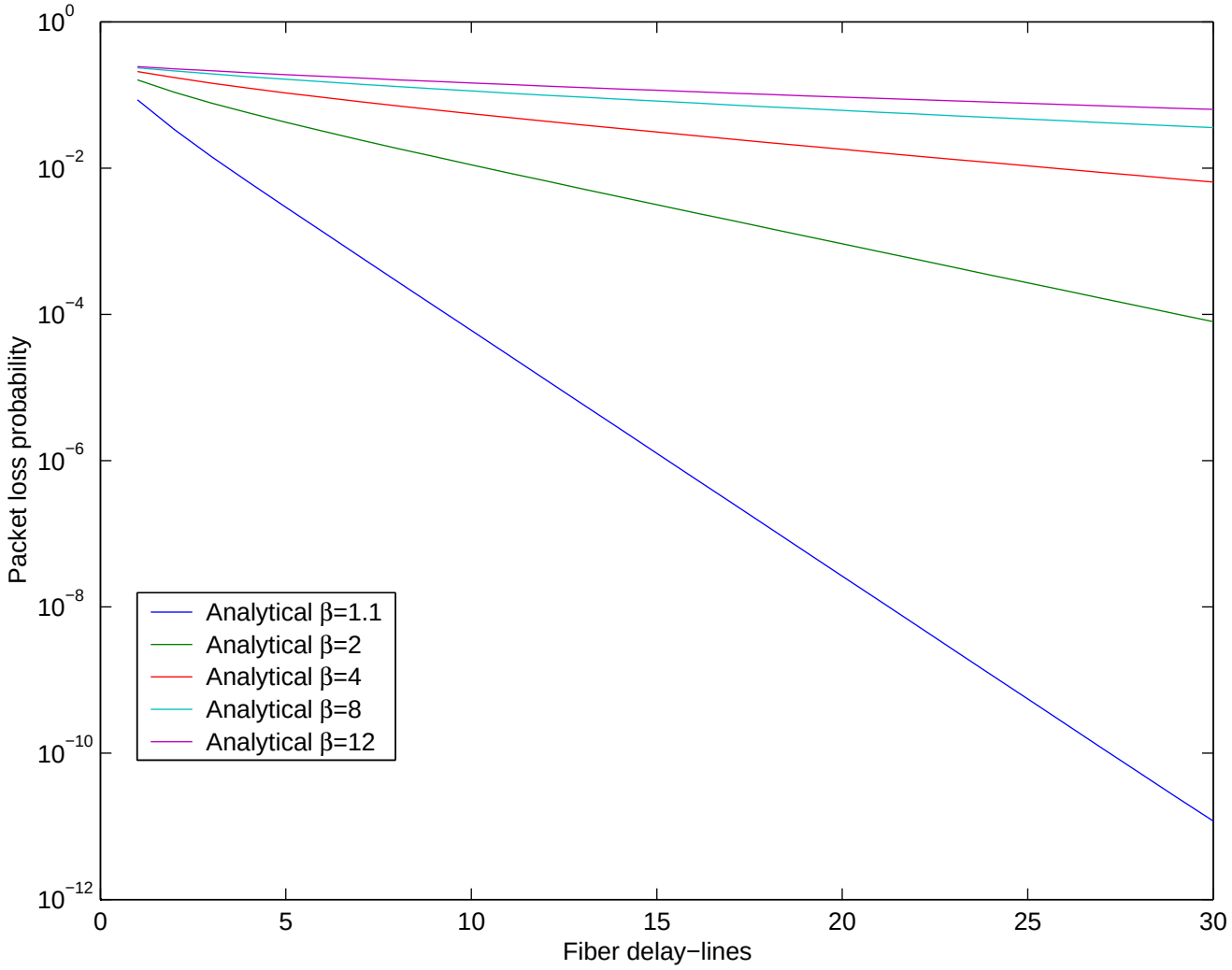

Figure 3.23: Packet Loss Probability versus buffer depth using burstiness as a variable parameter: load per channel 0.8

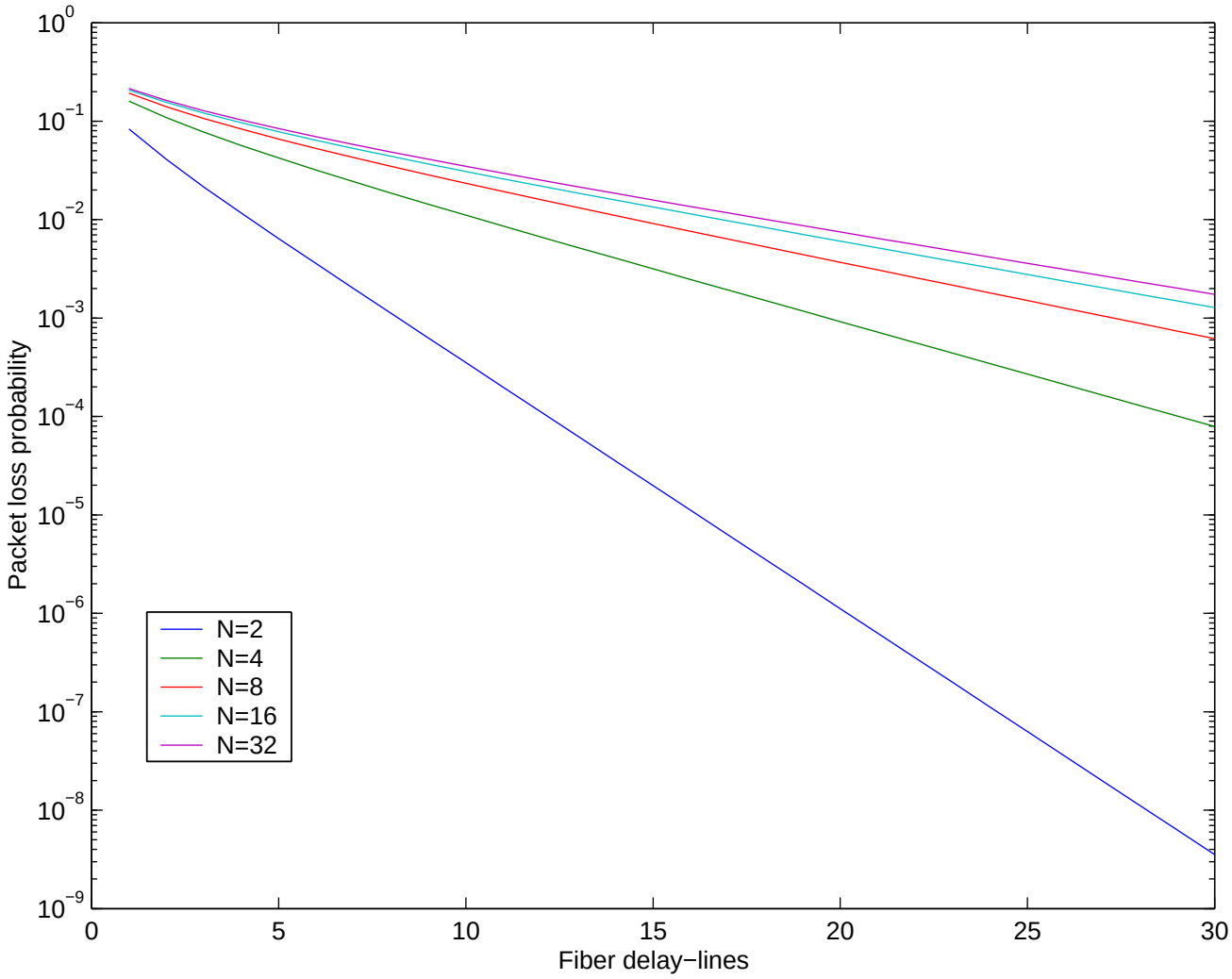

Figure 3.24: Packet loss probability versus buffer depth using switch size as parameter under offered load 0.8: Burstiness=2

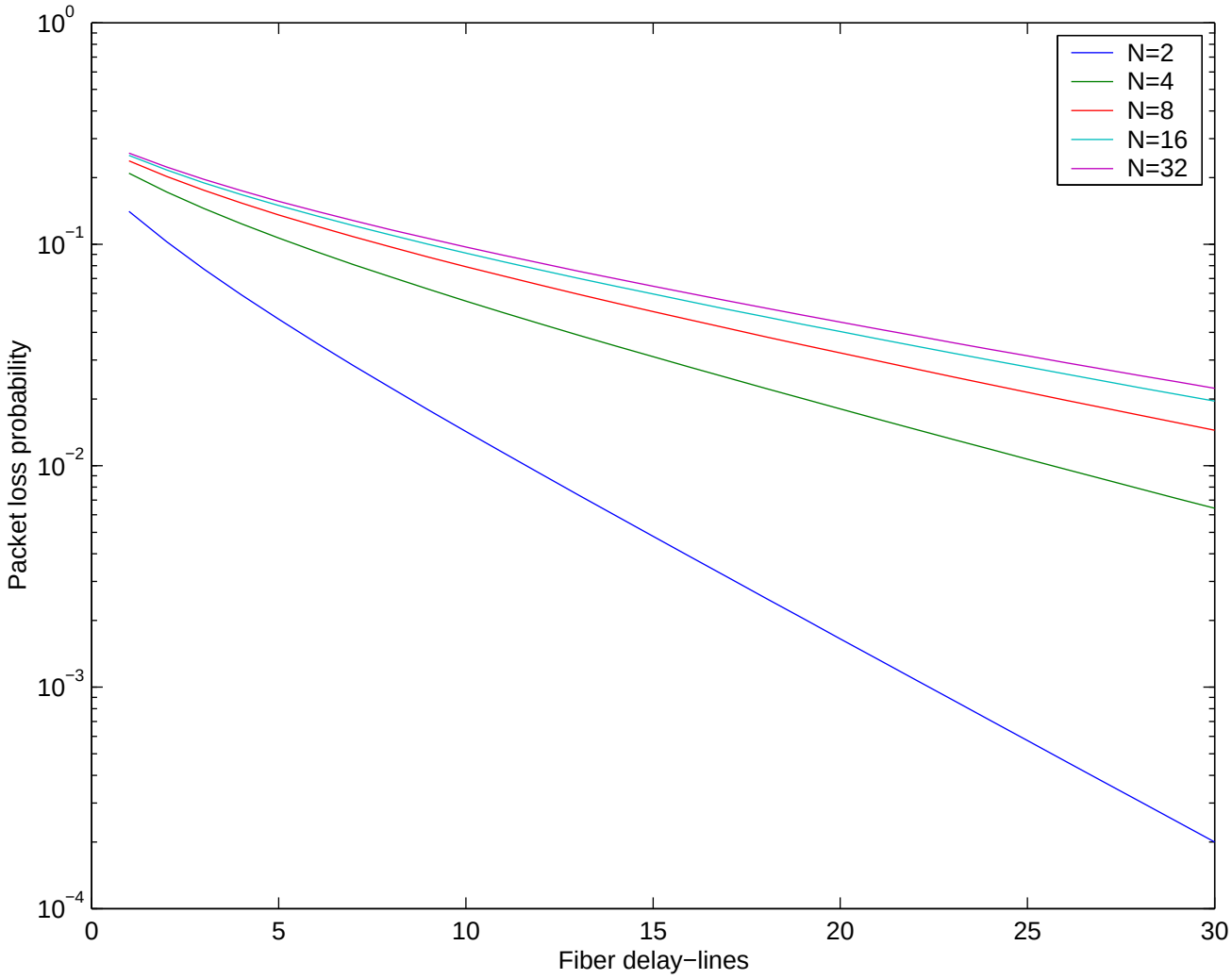

Figure 3.25: Packet loss probability versus buffer depth using switch size as parameter under offered load 0.8: Burstiness=4

Chapter 4

Correlated and Non-uniform traffic Optical Router Model

Now we consider correlated and, input/output non-uniform traffic. Non-uniform input traffic means that traffic is not evenly distributed among sources, while non-uniform output traffic is related to the fact that output links may have different probabilities of being selected by sources, which is given by routing probabilities in the matrix traffic. A similar model is given in [27], which deals with an electronic router having speed-up constraints for the number of packet sources that can be gathered by the switch. Instead, we consider an optical router that doesn't have such a constraint, and introduces WDM.

4.1 Introduction

Router architectures with output buffering have optimum throughput performance. Switch fabrics with only input buffering, limit the maximum throughput of the switch.

The input traffic to nodes is usually a multiplexed traffic from several previous sources and thus can be modelled by an uncorrelated (random) traffic. This modelling is especially appropriate when the speed of the sources is lower than the line speed of the router. In this case two adjacent cells of the same source may appear far apart (uncorrelated). However, if the speed of the sources is comparable to the line speed of the router, then the random assumption may not be appropriate, for optical routers there is no such limitation of line speed. In this case, correlated traffic is assumed.

Each input traffic process is modelled as an Interrupted Bernouli Process (IBP). This traffic model captures some traffic characteristics such as burstiness and ON/OFF activity periods. The traffic sources may have different traffic parameters and different routing probabilities. The imbalanced loading assumption models real situations.

We use a decomposition and aggregation process. We analyze node performance, while allowing

imbalanced traffic sources modelled by IBPs, where all cells that belong to a burst are routed to the same output queue. Imbalanced output loading is also assumed.

4.2 Router and traffic model

We are considering a discrete-time model of an optical router. The router is a nonblocking NxN, and each output port has a dedicated queue of size B cells, each input fiber contains z wavelengths for carrying a packet each wavelength. The time is slotted in units of cell service time. The switch fabric selects all cells with the same output address and places them at their output buffer in one time slot. A cell leaves its queue after receiving service of one time slot duration. Cells are serviced according to the first-in-first-out (FIFO) strategy. A cell arriving at a queue which is full will be lost. Each input traffic source $i, i = 1, ..., zN$, is modelled by an interrupted Bernoulli process (IBP_i) with parameters α_i and β_i as shown in Figure 4.1.

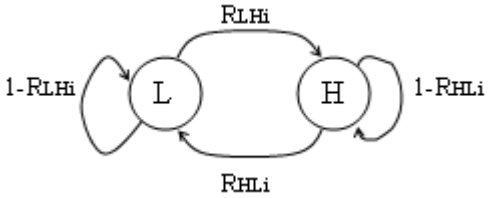

Figure 4.1: Markov chain describing the input traffic for source i.

The IBP alternates between two time periods. During a silence period no packets arrive at the inputs. During an active period packet arrive in every time slot. The steady-state probability that any slot contains a packet ρ_i is given by

$$\rho_i = \frac{\bar{\beta}_i}{\bar{\beta}_i + \bar{I}_i} \tag{4.1}$$

where $\bar{\beta}_i$ is the mean burst length ($= 1/R_{HLi}$) and $\bar{I}_i$ is the mean idle period ($= 1/R_{LHi}$). Mean burst length or burstiness index of the input traffic is also denoted by $r_b(i)$.

4.3 Model analysis by aggregation

Since we consider a completely partitioned output buffer, we can look at a particular output buffer, say 1. The state of the discrete-time queueing model of the buffer is described immediately after the beginning of each time slot by the vector $(\omega; n_1) = (\omega_1, \ldots, \omega_{zN}, n_1)$ where $w \in S_w$ is a vector describing the state of the zN arrival processes and n_1, is the number of cells in output buffer $1; O \leq n_1 \leq B$. w_i is a subvector (x_i, y_i) where x is the activity state of the ith arrival source and y is the destination port of the burst. $x\epsilon\{0, 1\}$; state 0 represents a silence and state 1 represents a burst. $y\epsilon\{1, 2. \ldots, N\}$.

In the following we describe the procedure for generating W, the transition matrix of the vector ω. Let Q_i be the transition matrix of the ith arrival process. $W(\omega^a, \omega^b)$ is the transition probability from state $\omega^a = ((x_1^a, y_1^a), \ldots, (x_{zN}^a, y_{zN}^a)$ to the state $\omega^b = ((x_1^b, y_1^b), \ldots, (x_{zN}^b, y_{zN}^b)$. Then, with the assumption that the zN arrival processes are independent, $W(\omega^a, \omega^b)$ can be calculated by using the following equation

$$W(\omega^a, \omega^b) = \prod_{i=1}^{zN} Q_i((x_i^a, y_i^a), (x_i^b, y_i^b)) \tag{4.2}$$

where for $1 \leq j, k \leq N$

$$Q_i((1,j),(1,j)) = 1 - R_{HLi} \tag{4.3}$$

$$Q_i((1,j),(0,j)) = R_{HLi} \tag{4.4}$$

$$Q_i((1,j),(1,y)) = 0, \quad y \neq j \tag{4.5}$$

$$Q_i((0,j),(0,j)) = 1 - R_{LHi} \tag{4.6}$$

$$Q_i((1,j),(1,k)) = R_{LHi} d_{ik} \tag{4.7}$$

Note that $\pi_w[(\omega)]$, the steady-state probability of state (ω), can be obtained by

$$\pi_W(\omega) = \prod_{i=1}^{zN} \pi_i[(x_i, y_i)] \tag{4.8}$$

where $\pi_i(x_i, y_i)$ is the steady state of (x_i, y_i) for the ith source, so $\pi(0,j) = (1 - \rho_i d_{ij})$ and $\pi_i(1,j) = \rho_i d_{ij}$ for $i\epsilon\{1, 2, \ldots, zN\}$ and $j\epsilon\{1, 2, \ldots, N\}$. This forces all cells in a burst to be switched to the same output queue.
The state space associated with one output buffer can be reduced by aggregating the zN arrival processes, as defined by the transition matrix W, into one arrival process, with transition matrix W^*. The state space of the aggregated arrival process is $k, k = 0, 1, \ldots, zN$. If the aggregated arrival process is in state $k = i$, then there are i cells arriving at output buffer j. For simplicity we may assume j = 1.

The transition matrix W^* of the aggregated process can be induced from W as follows: let S_w be the state space associated with W, and let S_{w^*}. be the aggregated state space. Then each state in S_{w^*}, say $k = i$, represents the aggregation of all states in S_w with exactly i arrivals destined to queue j. The transition probability, $W^*(i, i')$, between state i and state i' in the induced space can be calculated from

$$W^*(i, i') = \frac{\sum_{\omega^a \epsilon G} \pi(\omega^a) \sum_{\omega^b \epsilon G'} W(\omega^a, \omega^b)}{\sum_{\omega^a \epsilon G} \pi(\omega^a)} \tag{4.9}$$

where $G = \{\omega^a; f_j(\omega^a) = i\}, G' = \{\omega^b; f_j(\omega^b) = i'\}$ where f_j denotes the map from S_w to S_{w^*} such that $f_j(\omega^a) = k, k \leq zN$, if k bursts are directed to output port j. The steady-state probability of a state k in the induced space is given by

$$\pi_W^*(k) = \sum_{\omega^a \epsilon G} \pi_W(\omega^a) \tag{4.10}$$

The state of the output buffer j driven by the aggregated source can now be described by (k, n), where k is the number of cells arriving to the queue j immediately after the beginning of the slot and n is the queue length of queue j at that time. We assume that the service time is one slot and that arrivals have to wait one slot before service starts. The queue length immediately after the end of the slot is therefore $min\{(n-z,0)^+ + k, B\}$. The transition probability between any two states of the queue and the aggregated source is

$$P^*((k,n);(k',n')) = W^*(k,k')\chi\{n' = min\{(n-z,0)^+ + k, B\}\} \tag{4.11}$$

where (k', n') is the state of queue j in the next slot and χ. is an indicator function. P^* is a transition matrix for the state space $\{(k,n) : 0 \leq k \leq zN, 0 \leq n \leq B\}$.

Once W^* has been found, the steady-state probabilities $\Pi^*(k,n)$ of the queue driven by the aggregated process can be obtained by numerically solving the linear system of equations $\pi^* P^* = \pi^*$.

4.4 Router Performance

The cell loss probability defined as the ratio between the expected number of lost cells and the expected total number of arrivals, can be obtained by

$$P_{loss} = 1 - \frac{C_1 - C_2}{C_3} \tag{4.12}$$

where C_1 is the expected number of cells accepted by the switch fabric and destined to output j. C_2 is the expected number of cell losses due only to finite buffer. C_3 equals to traffic load. $C_1 = \sum_k \sum_n k\Pi^*(k,n)$ and $C_2 = \sum_k \sum_n [max(n-z,0) + k - B]^+ \pi^*(k,n)$. The queue length distribution $\pi^*(n)$ can be found from $\pi^*(k,n)$ summing over all k's.

Figure 4.2 shows the Packet loss probability at three output links for a router with traffic load $\rho_i = 0.9$, burstiness= 4, number of delay lines from 1 to 10, and routing probabilities given bellow

0.35	0.45	0.2
0.333	0.333	0.333
0.25	0.25	0.5

Figure 4.3 shows the Packet loss probability at traffic load of 0.5. As we can see, the number of delay lines is reduced when the packet loss probability increases, and viceversa. The greater the traffic load the greater the number of delay lines, in order to maintain a certain packet loss probability.
Here we showed small values of N and n because the high memory space and amount of calculations required in order to compute packet loss probability, i.e. W matrix has dimensions of $(2N)^{nN} x (2N)^{nN}$.

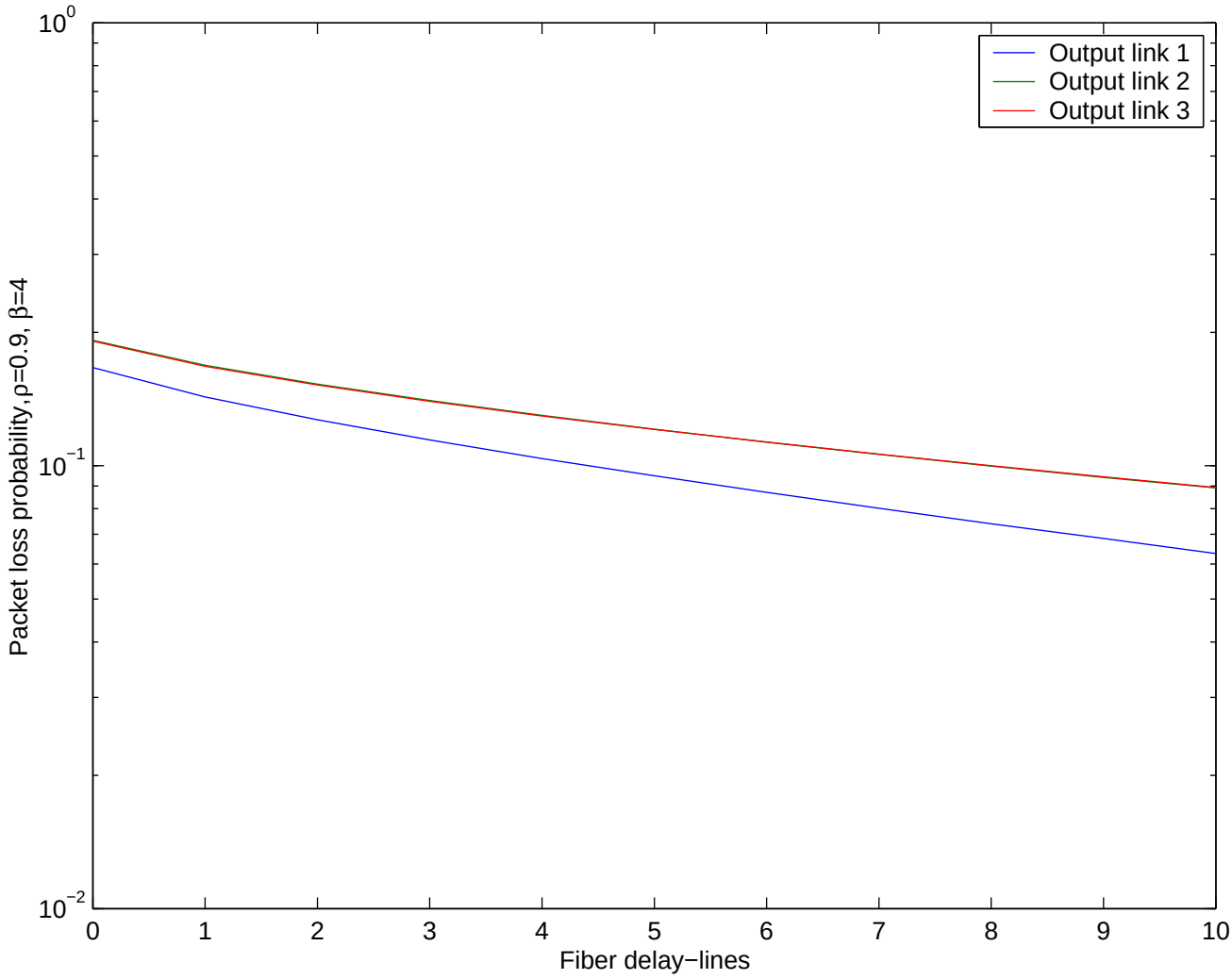

Figure 4.2: Packet loss probability under correlated and non-uniform traffic versus number of delay lines for load=0.9

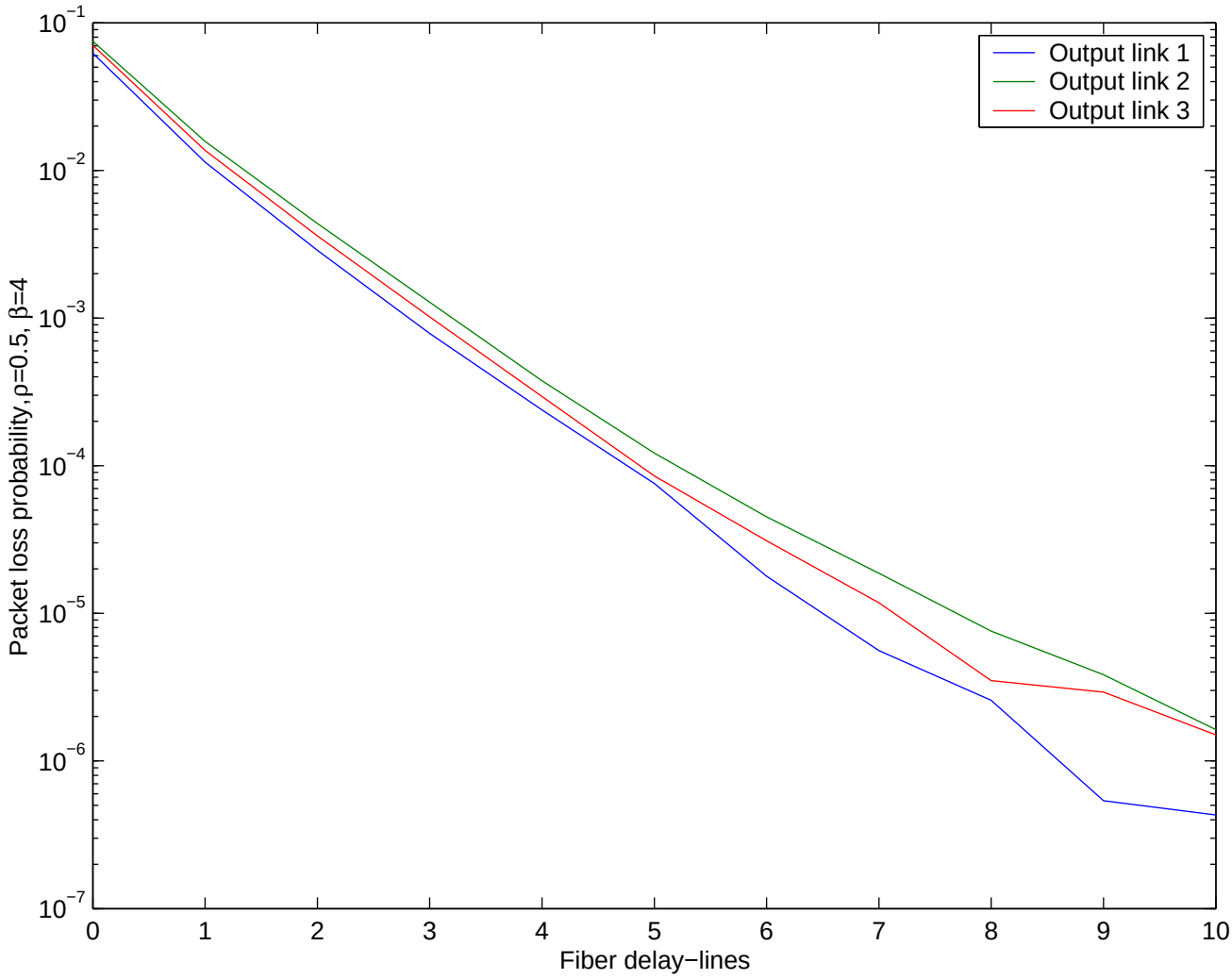

Figure 4.3: Packet loss probability under correlated and non-uniform traffic versus number of delay lines for load =0.5.

Chapter 5

Conclusions and Future work

An extensive study into the traffic features of a convenient analytical model to be applied to time-slotted output-buffered photonic nodes was performed. Statistical tools were developed, in an analytical framework, allowing comparisons with self-similar traffic. It is important to highlight that this model may evaluate node performance under more strict conditions than by using the so-called self-similar models. The improvements achieved by exploiting the wavelength domain in photonic packet switching were demonstrated through analytical models considering both random and correlated (on-off) traffic. WDM enable switch capacity multiplication and reduction in buffer depth.

When correlated traffic is considered, required elements (channels number, router optical memory, routers number) in a network increases with respect to that of independent traffic. Performance degradation is present when due to marginal distribution as correlation span appears to reach a saturation level, for the range of interest, after the aggregation of many sources is performed. In order to maintain a packet loss probability, the number of delay lines must be increased if burstiness is increased, and viceversa. If we have a fixed memory size, when burstiness increases, the packet loss probability decreases and viceversa.

The results also showed that hot-spot traffic largely affects the switch performance.

The models here analyzed have shown to be accurate, and they provide us useful models to analyze buffer performance with memoryless sources that introduces Short-Range Dependence for input and output non-uniform traffic.

As future work, it must be considered a model that deals with Long Range Dependence, by means of sources with long memory and Heavy-Tailed distributed, in order to evaluate buffer performance in optical routers.

Bibliography

[1] J. Beran, *Statistics for long-memory processes*, Chapman and Hall, New York, 1994

[2] A. Bononi, G. Castañón, O. K. Tonguz, "Analysis of hot-potato optical networks with wavelength conversion", *J. Lightwave Technol.*, vol. 17, pp. 525-534, Apr. 1999.

[3] A. Borella, F. Chiaraluce, F. Meschini, , "Statistical Multiplexing of Random Process in Packet Switching Networks", *IEE, Proc. Commun.* Vol. 143. No 5, pp. 325-334, Oct. 1996

[4] F. Callegati, M. Casoti, C. Rafaelli, "Packet optical network for highspeed TCP-IP backbones", *IEEE Commun. Mag.*, vol. 37, pp. 124-129, Jan. 1999.

[5] G. Castañón, "Design-Dimensioning Model for Transparent WDM Packet-Switched Irregular Networks", *Journal of Linghtwave Technology*, vol. 20, No. 1, Jan. 2002.

[6] G. Castañón, L. Tancevski, L. Tamil, "Optical packet switching with multiple path routing", *Comput. Networks* ISDN J., vol. 32, pp. 653-662, May 2000.

[7] G. Castañón, O. K. Tonguz, A. Bononi, "On the benefits of wavelength translation in datagram all-optical networks", *Electron. Lett.*, vol. 33, pp. 1567-1568, Aug. 1997.

[8] G. Castañón, L. Tancevski, L. Tamil, "Routing strategies for the optimization of components in all-optical packet switched networks", in *Proc. ECOC99*, vol. 1, Sept. 26-30, 1999, P4.1, pp. 420-421.

[9] G. Castañón, L. Tancevski, S. Yagnanarayanan, L. Tamil, "Asymmetric WDM all-optical packet switched routers", in *Proc. OFC2000*, Mar. 2-10, 2000, WD4-1, pp. 53-55.

[10] S. L. Danielsen, B. Mikkelsen, C. Joergensen, T. Durhuus, K. E. Stubkjaer, "WDM packet switch architectures and analysis of the influence of tuneable wavelength converters on the performance", *J. Lightwave Technol.*, vol. 15, pp. 219-226, Feb. 1997.

[11] S. L. Danielsen, C. Joergensen, B. Mikkelsen, K. E. Stubkjaer, "Optical packet switched network layer without optical buffers", *IEEE Photon. Technol. Lett.*, vol. 10, pp. 896-898, June 1998.

[12] F. Forghieri, A. Bononi, P. Prucnal, "Analysis and comparison of hot-potato and single-buffer deflection routing in very high bit rate optical mesh networks", *IEEE Trans. Commun.*, vol. 43, pp. 88-98, Jan. 1995.

[13] M. Grossglauser and J-C Bolot, "On the relevance of long-range dependence in network traffic", *Trans. on Networking*, Vol. 7, No. 5, pp. 629-640, Oct. 1999.

[14] K. M. Guild and M. J. O'Mahony, "Routing and buffering architecture in all-optical networks", *Electronic Letters*, vol. 35. n. 02, Jan. 1999.

[15] H. Heffes and D. M. Lucantoni, "A Markov modulated characterization of packetzed voice and data traffic and reated statistical multiplexer performance", *IEEE Journal on Selected Areas in Comm.*, Vol. SAC-4, No. 6, pp. 856-867, Sep. 1986.

[16] H. Heffes, "A class of data traffic processes-covariance function characterization and related queuing results", *Bell system tech. journal*, Vol. 59, No. 6, pp. 897-929, July-Aug. 1980.

[17] D. Heyman and T. Lakshman, "What are the implications of long-range dependence for VBR-video traffic engineering", *IEEE/ACM Transactions on Networking*, 4(3) pp.301317, June 1996.

[18] M. G. Hluchyj, M. J. Karol, "Queueing in high-performance packet switching", *IEEE J. Select. Areas Commun.*, vol. 6, pp. 1587-1597, Dec. 1988.

[19] T-C. Hou, and A. K.Wong, "Queueing Analysis for ATM Switching of Mixed Continuous-Bit-Rate and Bursty Traffic", In *Proc. INFOCOM90*, Vol..2, pp. 660-667, 1990.

[20] T-C. Hou and D. M. Lucantoni, "Buffer sizing for synchronous self-routeing broadband packet switches with bursty traffic", *Int. Journal of Digital and Analog Cabled Systems*, Vol. 2, pp 253-260, (1989).

[21] F. Huebner, D. Liu and J. M. Fernandez, "Queueing Performance Comparison of Traffic Models for Internet Traffic", In *Proc. of Globecom 98*, pp 471476, 1998.

[22] I. Ide, "Superposition of interrupted poisson processes and its application to packetized voice multiplexers", in *Proc. ITC89(ITC-12)* pp1399-1405, 1989.

[23] R. Jain and S. Routhier, "Packet trains-measurements and a new model for computer network traffic", *IEEE J. Select. Areas Commun.*, Vol..4, No. 6, 986995, Jun.1986.

[24] W. E. Leland, M. S. Taqqu, W. Willinger, D. V. Wilson, "On the Self-Similar Nature of Ethernet Traffic (Extended Version)", *IEEE/ACM Transactions on Networking*, vol. 2, No. 1, Feb. 1994.

[25] W. E. Leland, and D. V. Wilson, "High Time Resolution Measurements and Analysis of LAN Traffic: Implications for LAN Interconnection", *Proc. INFOCOM91*, vol.3, pp. 1360-1366,1991.

[26] A. León-García, *Probability and Random Processes for Electrical Engineering*, 2nd Ed. Addison Wesley, 1994

[27] I. I. Makhamreh, N. D. Georganas and D. McDonald, "Analysis of an output-buffered ATM switch with speed-up constrains under correlated and imbalanced bursty traffic", *IEE Proc. Communications* Vol. 142, No. 2, pp. 61-66, April 1995

[28] R. Nelson, *Probability Stochastic Processes, and Queueing Theory*, Spring-Verlang, New York, 1995.

[29] I. Noros, J. W. Roberts, A. Simonian, and T. Virtamo, "The superposition of variable bit rate in ATM multiplexer", *IEEE Journal of Selec. Areas in Comm.*; Vol. 9, No. 3, pp. 378-387, April 1991

[30] K. Park and W. Willinger, *Self-similar network traffic: an overview, in self-similar network traffic and performance evaluation*, Ch. 1, edited by K. Park and W. Willinger, Wiley, 2000.

[31] K. Park, G. Kim, and M. Crovella, "On the effect of traffic self-similarity on network performance", *Technical Report CSD-TR 97-024* Dept. of Computer Sciences Purdue University,1997

[32] V. Paxson and S. Floyd, "Wide-area traffic: the failure of Poisson modeling", *IEEE/ACM Transactions on Networking 3*, pp. 226-244, 1995.

[33] V. Paxson, "Fast approximation of self-similar network traffic", *Computer Communications Review*, Vol. 27, N. 5, pp. 5-18, October1997.

[34] M. R. N. Ribeiro, *Traffic Prioritisation in Photonic Packet Switching*, Ph.D. Thesis, University of Essex, June 2002.

[35] M. R. N. Ribeiro, M. J. OMahony, "On prioritization and optical buffer management in photonic packet switching nodes", in *Proc. OFC 2000*, Mar. 2-10, 2000, ThU2-1, pp. 289-291.

[36] T. G. Robertazzi, *Computer Networks and Systems, Queueing Theory and Performance Evaluation*, 2nd Ed.

[37] B. K. Ryu, and A. Elwalid, "The importance of long-range dependence of VBR video traffic in ATM traffic engineering: myths and realities", In *Proc. SIGCOMM96*, pp. 3-14, 1996. 56

[38] J. Shaikh, J. Rexford, and K. Shin, "Load-sensitive routing of long-lived IP flows", In *Proc. ACM SIGCOMM99*, pp. 215226, 1999.

[39] K. Sohraby, "On the theory of general on-off sources with applications in high-speed networks", In *Proc. INFOCOM93*, Vol. 2, pp. 401-410, 1993.

[40] T. Tarongí, D., D. Rodellar, J. M. Torner, J. Solé-Pareta, S. Borgione, "Traffic characterization using optical based packet switches with Poisson and fractal traffic sources", In *Proc. ONDM 01*,. 2001

[41] W. Willinger, M. S. Taqqu, R. Sherman, D. V. Wilson, "Self-Similarity Through High-Variability: Statistical Analysis of Ethernet LAN Traffic at the Source Level", *IEEE/ACM Transactions on Networking*, VOL. 5, NO. 1, pp. 71-86, Feb. 1997.

Appendix A

Demonstrations

A.1 Proof of equation (2.17)

Equation (2.17) is shown below

$$var[\Theta_i] = var[X_i]\{m + \sum_{k=1}^{m-1}(m-k)[(k+1)^{2H} - 2k^{2H} + (k-1)^{2H}]\} = var[X_i]m^{2H}$$

Looking into the terms within the summation one can observe the following pattern:

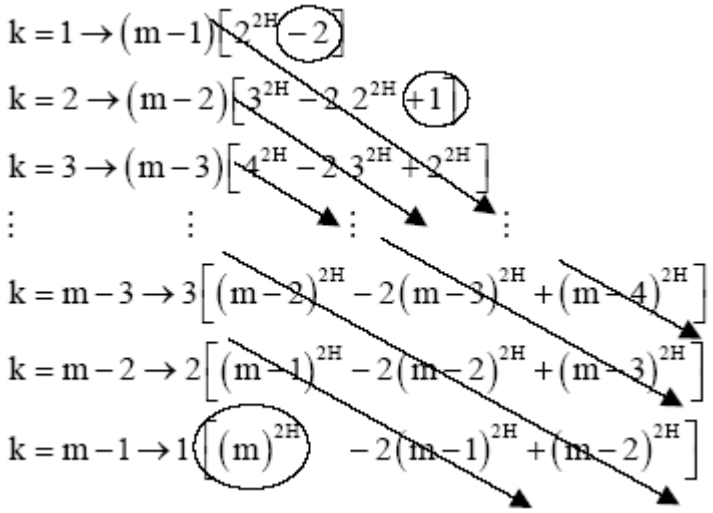

Notice that each base only appears at most in three values of k since $k+1$, k, and $k-1$. Terms with same base cancel each other when multiplied by $(m-k)$ and added, except for the ones within circles. Therefore the summation is reduced to

$$m^{2H} - 2(m-1) + (m-2) = m^{2H} - m$$

By adding the term of out the summation in 2.11 one finally obtains

$var[Xi]m^{2H}$

A.2 Proof of Equation (3.2)

Considering steady state probabilities, and observing for balance equations we have

$$\sum_j P_{ij} = 1$$

so, $R_{LL} = 1 - R_{LH}$ and $R_{HH} = 1 - R_{HL}$

as $n \longrightarrow \infty$,

$P_{ij}(n) \longrightarrow \pi_j \qquad \forall i$

$\Pi = \{\pi_j\}$ and $\sum_i \pi_i = 1$

$\pi_j = \sum_i P_{ij}\pi_i$

$$\begin{matrix} 1 - R_{LH} & R_{LH} \\ R_{HL} & 1 - R_{HL} \end{matrix}$$

then

$\pi_L = P_{00}\pi_L + P_{10}\pi_H$

$\pi_H = P_{01}\pi_L + P_{11}\pi_H$

and

$\pi_L + \pi_H = 1$

solving the above equation system we finally obtain

$\pi_H = \frac{R_{LH}}{R_{LH}+R_{HL}}$

A.3 Proof of Equation (3.4)

Following the steps described in [20] we can see that:

$$Q_{ij} = Prob[S(T+1) = S_j | S(T) = S_i]$$

$$= I_{(j \geq i)} \sum_{k=j-i}^{min(N-i,j)} [\binom{N-i}{k} R_{LH}^{k} (1 - R_{LH})^{N-i-k}$$

$$\binom{i}{k-j+i} R_{HL}^{k-j+i} (1 - R_{HL})^{j-k}]$$

$$+ I_{(j<i)} \sum_{k=i-j}^{min(i,N-j)} [\binom{i}{k} R_{HL}^{k} (1 - R_{HL})^{i-k}$$

$$\binom{N-i}{k-i+j} R_{LH}^{k-i+j} (1 - R_{LH})^{N-k-j}]$$

$$= \sum_{k=max(0,i-j)}^{min(i,N-j)} [\binom{i}{k} R_{HL}^{k} (1 - R_{HL})^{i-k}$$

$$\binom{N-i}{k-i+j} R_{LH}^{k-i+j} (1 - R_{LH})^{N-k-j}]$$

where

$$I_{(x)} = \begin{cases} 1 & \text{, if x is true} \\ 0 & \text{, otherwise} \end{cases}$$

A.4 Proof of convergence of Equation (3.13)

$NV(m) = \frac{1}{m^2}[m + 2\sum_{u=1}^{m-1}(m-u) r_A(u)]$

For $r_A(u) = 0$ and $u > 1$ it is easily seen that

$NV(m) = \frac{1}{m}$

For $r_A(u) = 1$ and $u > 0$ the summation becomes

$\sum_{u=1}^{m-1}(m-u) = \sum_{u=1}^{m-1} m - \sum_{u=1}^{m-1} u = m(m-1) - \frac{(m-1)(m)}{2} = \frac{(m)(m-1)}{2}$

Above is done, taking into account:

$\sum_{i=1}^{n} i = \frac{n(n+1)}{2}$

Therefore, one has the following result

$NV(m) = \frac{1}{m^2}[m + \frac{2(m-1)m}{2}] = 1$